The role of radiation in organizing convection in weak temperature gradient simulations

Sharon L. Sessions,[1] Stipo Sentić,[1] and Michael J. Herman,[1]

Corresponding author: S. L. Sessions, Department of Physics and Geophysical Research Center, New Mexico Institute of Mining and Technology, 801 Leroy Pl., Socorro, NM 87801, USA. (sessions@kestrel.nmt.edu)

[1]Department of Physics and Geophysical Research Center, New Mexico Tech, Socorro, NM, USA.

Abstract.

Using a cloud system resolving model with the large scale parameterized by the weak temperature gradient approximation, we investigated the influence of interactive versus non-interactive radiation on the characteristics of convection and convective organization. The characteristics of convecting environments are insensitive to whether radiation is interactive compared to when it is not. This is not the case for non-convecting environments; interactive radiative cooling profiles show strong cooling at the top of the boundary layer which induces a boundary layer circulation that ultimately exports moist entropy (or analogously moist static energy) from dry domains. This upgradient transport is associated with a negative gross moist stability, and it is analogous to boundary layer circulations in radiative convective equilibrium simulations of convective self-aggregation. This only occurs when radiation cools interactively. Whether radiation is static or interactive also affects the existence of multiple equilibria–steady states which either support precipitating convection or which remain completely dry depending on the initial moisture profile. Interactive radiation drastically increases the range of parameters which permit multiple equilibria compared to static radiation; this is consistent with the observation that self-aggregation in radiative-convective equilibrium simulations is more readily attained with interactive radiation. However, the existence of multiple equilibria in absence of interactive radiation suggests that other mechanisms may result in organization even in absence of interactive radiation.

1. Introduction

Convective organization is the phenomenon in which convection forms coherent structures, usually flanked by dry subsiding regions in the troposphere. It is important since the spatio-temporal distribution of convection and moisture has a significant impact on the global energy budget. Organized convection modulates the amount of energy radiated upward in clear sky regions compared to the longwave radiation that is trapped by water vapor. As the atmosphere warms, there is evidence for an increased tendency for convection to organize. This may act as a negative feedback that cools the atmosphere as the climate changes [*Khairoutdinov and Emanuel*, 2010]. Understanding the mechanisms which control the large-scale organization of tropical deep convection not only helps to prepare for the consequences of climate change, but provides important clues for improving parameterizations of these processes in large scale models.

The mechanisms thought to be responsible for organizing convection are as diverse as the various manifestations of organization; the latter include tropical cyclones, convectively coupled waves, and the Madden-Julian Oscillation among others. Observations and numerical experiments have identified several important factors in convective organization. These include interaction with tropical waves [*Frank and Roundy*, 2006; *Kiladis et al.*, 2009], cloud-radiation interactions [*Tompkins and Craig*, 1998; *Nilsson and Emanuel*, 1999; *Raymond*, 2001; *Bretherton et al.*, 2005; *Nolan et al.*, 2007; *Muller and Held*, 2012; *Wing and Emanuel*, 2013], sea surface temperature (SST) distributions [*Lindzen and Nigam*, 1987; *Tompkins*, 2001a, b; *Nolan et al.*, 2007; *Back and Bretherton*, 2009], convection-moisture feedbacks [*Held et al.*, 1993; *Tompkins*, 2001b; *Craig and Mack*, 2013], horizontal moisture advection [*Sobel et al.*, 2007; *Wang and Sobel*, 2012; *Sessions et al.*, 2015], mean surface wind [*Nolan et al.*, 2007], rotation [*Bretherton et al.*, 2005; *Nolan et al.*, 2007; *Khairoutdinov and Emanuel*, 2013; *Davis*, 2015], vertical wind shear [*Held et al.*, 1993; *Robe and Emanuel*, 2001; *Cohen and Craig*, 2006; *Anber et al.*, 2014], and cold pools [*Jeevanjee and Romps*, 2013; *Feng et al.*, 2015]. In addition, models also show that convective organization is sensitive to domain size [*Bretherton et al.*, 2005; *Nolan et al.*, 2007; *Muller and Held*, 2012], domain geometry [*Wing and Cronin*, 2015] model resolution [*Muller and Held*, 2012], and cloud microphysical parameterizations [*Bretherton et al.*, 2005], including the terminal velocity of raindrops [*Parodi and Emanuel*, 2009]. The thermodynamic environment is also important for convective organization as it may provide conditions which are either conducive or hostile to the development of deep convection [*Sessions et al.*, 2015]; an example of the former is cyclogenesis associated with temperature dipole anomalies in African Easterly Waves [*Raymond and Sessions*, 2007; *Gjorgjievska and Raymond*, 2014; *Raymond et al.*, 2015]. Convection may also organize in the absence of any obvious large-scale forcing. Spontaneous organization of convection in horizontally homogeneous forcing conditions is often refered to as "self-aggregation" [*Su et al.*, 2000].

The goal of this research is to consider the effect of interactive versus non-interactive radiation and the thermodynamic environment in organizing deep tropical convection. Rather than varying parameters and environmental conditions on a large domain, we implement a small domain cloud-system resolving model (CRM) which parameterizes the large-scale using the weak temperature gradient (WTG) approximation. The WTG approximation is based on the observation that horizontal temperature gradients are small in the tropical free troposphere as a result of the redistribution of buoyancy anomalies by gravity waves. WTG simulations have been used successfully to investigate various properties of convection and convective organization. For example, it has been implemented in a simple model of the Hadley circulation [*Polvani and Sobel*, 2002], the Madden-Julian Oscillation [*Wang et al.*, 2013; *Sentic et al.*, 2015], and cyclogenesis [*Raymond and Sessions*, 2007].

The WTG approximation has also been used as a computationally inexpensive method for investigating self-aggregation. Self-aggregation describes the phenomena by which convection spontaneously organizes into a single region exhibiting intense precipitation surrounded by an extremely dry, subsiding troposphere. It occurs on larger domains which are run to radiative-convective equilibrium (RCE). Multiple equilibria occur in certain smaller-domain WTG simulations in which a multiplicity of steady states arise that either support persistent precipitating convection, or else remain completely dry under identical forcing conditions [*Sobel et al.*, 2007; *Sessions et al.*, 2010; *Daleu et al.*, 2015a]. Multiple equlibria in WTG simulations are analogous to the dry and precipitating regions in larger self-aggregated RCE domains. Thus, WTG simulations may be used to investigate convective organization by identifying conditions which support or suppress domain-mean convection. Suppressing convection in WTG simulations is a proxy for organization since it represents the dry regions surrounding regions of active convection.

In addition to identifying conditions which support or suppress convection—and by analogy identifying relevant mechanisms of convective organization—WTG is also an efficient method for characterizing convection in different thermodynamic environments, as was demonstrated in *Sessions et al.* [2015]. In this work, we utilize the strategy of *Ses-*

sions et al. [2015], but rather than investigating the additional role of horizontal moisture advection [as in *Sessions et al.*, 2015], we consider how interactive versus non-interactive radiative cooling affects convection in different thermodynamic environments. Given that nearly all 3-dimensional RCE simulations of convective organization require interactive radiation for spontaneous organization [e.g. *Bretherton et al.*, 2005; *Muller and Held*, 2012]—the notable exception being *Tompkins* [2001b]—we hope to elucidate the role of interactive radiation in the organization of tropical convection. We will explicitly test this with multiple equilibria exeriments using interactive and non-interactive radiative cooling profiles and compare convective diagnostics with previous studies of self-aggregation.

The effect of interactive radiation compared to non-interactive radiation has been considered in previous WTG studies. *Anber et al.* [2014, 2015] investigated the convective response to vertical wind shear in WTG simulations. In the first paper, *Anber et al.* [2014] used a fixed radiative cooling rate of -1.5 K day^{-1}, while in the second paper they examined the role of interactive radiation compared to convection evolving with a static radiative cooling profile equal to the time and domain mean of the interactive case [*Anber et al.*, 2015]. The relevant results for this study are those relating to the unsheared cases. They found that interactive radiation produced much stronger vertical motion in the upper troposphere which imported low moist static energy air in the mid-troposphere. This resulted in an increase in normalized gross moist stability which decreased precipitation rate. As we illustrate below, our results contrast somewhat with these studies: we instead find that the interaction between radiation and the large-scale circulation occurs in the lower atmosphere. Precipitation rates as well as other convective diagnostics are insensitive to whether radiation is interactive. In contrast, non-precipitating steady states exhibit significant differences which affect convective organization.

This paper is organized as follows: In section 1.1, we briefly introduce the weak temperature gradient approximation and its implementation in our model. The model, different options for parameterizing radiative cooling, and numerical experiments are described in section 2. We characterize convection using several diagnostic quantities that are defined in section 3; results are presented in section 4. We discuss our results in the context of convective organization in section 5, and summarize our conclusions in section 6.

1.1. Weak temperature gradient (WTG) approximation

The weak temperature gradient (WTG) approximation provides a means to parameterize the large-scale tropical environment in limited domain simulations [*Sobel and Bretherton*, 2000; *Raymond and Zeng*, 2005]. We use an upgraded version of the model described in *Raymond and Zeng* [2005]; model upgrades are documented in *Herman and Raymond* [2014]. The procedure is similar to the experiments described in *Sessions et al.* [2015]; in that work, the authors investigated how different parameterizations of horizontal moisture advection affected the characteristics of convection using static radiative cooling profiles. Here, we choose to parameterize horizontal moisture advection using lateral entraiment induced by WTG circulations (described below), and consider the effect of interactive versus non-interactive radiative cooling.

The prognostic equation for equivalent potential temperature, θ_e is:

$$\frac{\partial \rho \theta_e}{\partial t} + \nabla \cdot (\rho \mathbf{v} \theta_e - K \nabla \theta_e) = \rho (S_{es} + S_{er} - S_e), \tag{1}$$

where ρ is the density, $\mathbf{v}$ is the velocity, and K is the eddy mixing coefficient. S_{es} and S_{er} are sources of equilvalent potential temperature from surface fluxes and radiation; S_e is the sink of θ_e due to enforcing the WTG approximation.

The total water mixing ratio, r_t, is governed by:

$$\frac{\partial \rho r_t}{\partial t} + \nabla \cdot (\rho \mathbf{v} r_t - K \nabla r_t) = \rho S_{cr} + \rho (S_{rs} - S_r) \quad . \tag{2}$$

Here, S_{cr} is minus the conversion rate of cloud water to precipitation, S_{rs} is the source of total cloud water from surface evaporation, and S_r is a sink of total water mixing ratio that results from enforcing the WTG approximation.

The WTG approximation is enforced by relaxing the domain mean potential temperature, $\overline{\theta}$, to a reference profile which represents the large-scale, θ_0, over a time scale t_θ. This results in a potential temperature sink, S_θ:

$$S_\theta = M(z) \frac{(\bar{\theta} - \theta_0)}{t_\theta}, \tag{3}$$

where $M(z) = \sin(\pi z / H)$ is a masking function which modulates the relaxation. It is only applied between the boundary layer top ($z = b$) and the tropopause ($z = H$); above H, M is set to zero.

The potential temperature anomaly in equation (3) generates a vertical velocity in the model—the weak temperature gradient vertical velocity—that counteracts the diabatic heating:

$$w_{wtg} = \left(\frac{\partial \bar{\theta}}{\partial z} \right)^{-1} S_\theta \quad . \tag{4}$$

This vertical velocity vertically advects moisture and, via mass continuity of the WTG velocity field, entrains moisture from the surrounding environment. This contributes to an external sink of total water mixing ratio (S_r in equation (2)):

$$S_r = w_{wtg}\frac{\partial \overline{r}_t}{\partial z} + (\overline{r}_t - r_x)\frac{1}{\rho_0}\frac{\partial \rho_0 w_{wtg}}{\partial z}, \qquad (5)$$

where the first term on the right side vertically advects moisture, and the second term laterally entrains moisture from the environment (specified by a reference profile r_{t0}) according to:

$$r_x = \begin{cases} \overline{r}_t & \text{if} \quad \partial \rho_0 w_{wtg}/\partial z < 0 \quad \text{(detraining levels)} \\ r_{t0} & \text{if} \quad \partial \rho_0 w_{wtg}/\partial z > 0 \quad \text{(entraining levels)} \end{cases}. \qquad (6)$$

Enforcing the WTG approximation also contributes to a θ_e sink (S_e in equation (1)) which is analogous to equations (5) and (6) with r_t replaced by θ_e.

We should also point out that since WTG is not a good approximation in the boundary layer, w_{wtg} is linearly interpolated from its value at the top of the boundary layer to zero at the surface.

2. Numerical Experiments

In this section we describe the model parameters, the reference profiles used in the implementation of WTG, and the options for radiatively cooling the model.

2.1. Model Set Up

The model set up in this study is identical to that used in *Sessions et al.* [2015] and is briefly described here for self-containment.

All simulations are performed on two-dimensional domains with a horizontal dimension 200 km and resolution of 1 km; the vertical spans 20 km with 250 m resolution. Two-dimensional domains are a good strategy for this work since the point is to understand the role of radiation in the response of convection to different thermodynamic environments. The sensitivity to changes in environments and model parameters is amplified in

2-dimensions compared to 3D [*Wang and Sobel*, 2011], so we can meet our objective using a computationally efficient approach.

WTG simulations typically require reference profiles for potential temperature (θ_0 in equation (3)) and mixing ratio (r_{t0} in equations (5) and (6)). These are obtained by time and domain averages of simulations run to radiative-convective equilibrium (RCE) in non-WTG mode ($t_\theta = \infty$ in equation (3)). The profiles in this work are averages over the last month of a one year long simulation; as discussed in *Sessions et al.* [2015], it is unnecessary to run the RCE simulation for 1 year, but we were investigating a continuous gradual warming in the model's stratosphere. This was attributed to a mass leak which we have confirmed did not affect the results of the WTG simulations (and which has since been fixed).

All simulations were run over an ocean with a surface temperature of 303 K. For RCE simulations, surface winds perpendicular to the model domain are relaxed to 5 m s^{-1}, and radiative cooling is permitted to adjust according to water vapor content in the domain (i.e., interactive radiation, described in more detail in section 2.3). The RCE profiles of potential temperature and total water mixing ratio are shown in figure 1.

In most WTG simulations, we increase the surface wind speed to 7 m s^{-1} to increase the convective response relative to the radiative cooling. For investigating multiple equilibria, we also consider wind speeds ranging from 3 to 10 m s^{-1} (described below). Radiative cooling is either static (time-independent) or interactive in the WTG simulations.

In implementing WTG, we must specify the time scale over which the domain mean potential temperature is relaxed to the reference profile (t_θ in equation (3)). Physically, t_θ represents the time scale over which gravity waves counteract buoyancy anomalies induced by convective heating. Typical values in WTG investigations are on the order of an hour [*Sessions et al.*, 2010; *Wang and Sobel*, 2011, 2012; *Daleu et al.*, 2012; *Anber et al.*, 2014; *Herman and Raymond*, 2014; *Wang et al.*, 2013; *Sentic et al.*, 2015], though some studies have used strict enforcement [$t_\theta = 0$, *Sobel and Bretherton*, 2000]. As in *Sessions et al.* [2015], we choose a relaxation time scale of approximately 11 min ($1/t_\theta = 1.5 \times 10^{-3}$ s^{-1}). We chose a shorter time scale than is typically implemented so that the modeled convection would be sufficiently sensitive to changes in the thermodynamic environment. Furthermore, *Sessions et al.* [2010] showed that shorter relaxation times permitted multiple equilibria over a larger range of wind speeds; thus the relaxation time chosen is conducive for investigating the effect of radiation treatment on multiple equilibria. While this is a convenient choice, it may also be physically reasonable. The relaxation time scale is believed to be related to the time over which gravity waves redistribute buoyancy anomalies. Gravity wave speed is set by the depth of convection [*Bretherton and Smolarkiewicz*, 1989], and 50 m s^{-1} is typical for deep convection. Given the gravity wave speed, the time scale is set according to the distance over which the gravity waves act. The appropriate distance is still an open question with assumptions ranging from the size of the convective cell [*Romps*, 2012a, b] to the distance between convective cells [*Bretherton and Smolarkiewicz*, 1989; *Cohen and Craig*, 2006]. A gravity wave traveling 50 m s^{-1} will travel 33 km in 11 min, which may be physically reasonable depending on what the appropriate length scale is.

2.2. Reference Profiles

As discussed in section 1, the thermodynamic environment can catalyze convective organization. We are interested in the convective response to changes in the thermodynamic environment, so we prescribe perturbations to the RCE reference profiles of potential temperature and mixing ratio (figure 1) to represent different environments. This is the same strategy used in *Sessions et al.* [2015]. The experiments were motivated by *Raymond and Sessions* [2007], who found that increasing the atmospheric stability by imposing a cooling of the lower troposphere and a warming aloft resulted in higher precipitation rates and more bottom-heavy convective profiles compared to unperturbed reference profiles; similarly, they found that moistening the lower troposphere resulted in higher precipitation rates with stronger convective profiles, but the shape of the convective profile remained unchanged. *Sessions et al.* [2015] expanded those basic perturbations to include perturbations of the opposite sign–less stable and drier–as well as all combinations of perturbations applied to reference moisture and potential temperature profiles. We use an identical strategy in this work for the reference profile perturbations; the difference is that we are considering different radiation treatments. In this work, horizontal moisture advection is parameterized by lateral entrainment associated with mass continuity in the WTG velocity field (see equations 5 and 6).

The perturbations that are added to the reference profiles of potential temperature and mixing ratio (figure 1) are shown in figure 2. They are arranged so that columns going left to right represent environments with increasing moisture (moisture perturbations are indicated with a dashed line), while rows going from the bottom to the top represent increasing atmospheric stability (potential temperature profiles are shown with a solid line). The center panel (figure 2e) represents the unperturbed environment. The symbols in the upper right of each panel are geometric representations of the atmospheric conditions:

1. upright triangles (geometrically more stable shapes) represent more stable θ profiles;

2. neutrally stable squares represent unperturbed θ profiles;

3. inverted triangles (geometrically unstable shapes) correspond to less stable θ profiles.

The shading corresponds to the moisture perturbations; in analogy with a glass of water:

1. empty is drier;

2. half-filled indicates unperturbed r_t profiles;

3. solid is moister.

We also use a bulls-eye to easily distinguish the case where neither θ or r_t is perturbed.

The perturbations shown in figure 2 are identical to those in *Raymond and Sessions* [2007] and *Sessions et al.* [2015]. Specifically, we add perturbations of magnitude $\Delta\theta$ at height h to the RCE θ profile, where $\Delta\theta$ is given by:

$$\Delta\theta = \delta\theta \left(\frac{z}{h}\right)^2 e^{[2(1-z/h)]} \quad , \tag{7}$$

where z is the altitude. More stable environments in figure 2 have $\delta\theta = -2$ K at $h = 3$ km and $\delta\theta = 2$ K at $h = 10$ km (cooling below and warming aloft); less stable environments add perturbations of the same magnitude with opposite signs. Moisture perturbations are given by a form identical to equation 7 but with $\delta\theta$ replaced by δr_t; $\delta r_t = \pm 1.0$ g kg^{-1} at $h = 3$ km.

As in *Sessions et al.* [2015], the experimental design prescribes a time dependent reference profile with the first month of the experiment given by the unperturbed RCE reference profiles, the second month perturbs *either* θ_0 or r_{t0}, and the third month perturbs *both* θ_0 and r_{t0}. All possible combinations and sequences of perturbations generate a complete representation of the environmental profiles represented by the perturbations in figure 2. The time dependent behavior in this work is very similar to the results shown in *Sessions et al.* [2015]; thus, we refer to that paper for details of time-dependent design and results (those details are not essential for the results presented here).

2.3. Radiative cooling options

The treatment of radiation in CRMs can have a significant impact on the modeled convection. For example, *Cohen and Craig* [2006] consider the effect of different radiative cooling rates on convective properties in RCE simulations; the magnitude of radiative cooling in these experiments was shown to affect the spatial distribution of convection. Large-scale RCE simulations also show that radiative cooling—whether it is fixed or else cools interactively with the thermodynamic state—has a major impact on the ability of convection in a model to organize [*Tompkins and Craig*, 1998; *Bretherton et al.*, 2005; *Muller and Held*, 2012; *Wing and Emanuel*, 2013; *Davis*, 2015].

We consider three options for radiation treatments:

1. fixed cooling rate of -1.8 K day^{-1} through the troposphere; this is the "fixed" option;

2. time-independent cooling profile generated from the RCE; since this option isn't at a fixed rate, but is static in time, we call this the "static" option;

3. interactive radiation in which the radiative cooling profile is calculated interactively by the model according to the column thermodynamics including the water vapor content; this is the "interactive" option.

The interactive radiation scheme uses an updated version of the toy model described in Raymond and Torres (1998). It calculates the radiative source term for equivalent potential temperature (S_{er} in equation 1) according to the net flux (upward stream minus downward stream) of infrared radiation. The spectrum of radiation is approximated by 11 water vapor bands (only six were used in Raymond and Torres 1998), one carbon dioxide band, and one band that accounts for atmospheric infrared windows and possible continuum absorption by water vapor. Radiative cooling is due to longwave radiation; shortwave radiation is not parameterized. Clouds increase absorptivity in proportion to cloud water content, and scattering is neglected. Though the approximations are significant, this computationally inexpensive scheme reproduced reasonable heating rates over a wide range of atmospheric conditions when it was compared to the National Center for Atmospheric Research CCM2 radiation model (see Raymond and Torres 1998 for further details of the radiation model).

The static radiative cooling profile eliminates the radiation interactions and thus isolates effects of radiation compared to other mechanisms, yet it maintains a cooling profile that is native to the model environment (it is given by the time and horizontal domain average of the interactive scheme over the last 30 days of the RCE simulation). On the other hand, many WTG simulations use a fixed radiative cooling profile (for example, see a recent intercomparison of large-scale parameterizations, including WTG, *Daleu et al.* [2015a]), and the shape of the cooling profile may also affect the characteristics of convection. Including both options can inform the extent to which the shape of the cooling profile affects convection (via its effect on the source of equivalent potential temperature, S_{er} in equation 1). We choose -1.8 K day^{-1} for the fixed option because this is the mean cooling rate of the radiative cooling profile in the troposphere calculated from the RCE simulation. In other words, vertically averaging the "static" radiative cooling profile in the lowest 15 km yields a net -1.8 K day^{-1}. Both the static and fixed cooling profiles are shown in each panel of figure 3 (these are unchanged across all thermodynamic environments).

Figure 3 shows the radiative cooling profiles for all choices of radiation treatment in all of the reference profiles represented by the perturbations in figure 2. Note that the static (blue) and fixed (black) profiles are–by design–independent of reference environment. Interactive radiation (red), on the other hand, is highly sensitive to changes in the reference potential temperature profile, but relatively insensitive to changes in the reference moisture profile. If the potential temperature is unperturbed (figure 3d-f), the interactive radiative cooling profile is nearly identical to the static cooling profile. In more stable environments (figure 3a-c), there is stronger cooling in the upper troposphere where the warm anomalies are prescribed, and less cooling in the lower troposphere where there are cool anomalies. In less stable environments (figure 3g-i), the interactive cooling profile changes drastically, with strong cooling in the boundary layer, and weak cooling aloft compared to the static cooling profile. The cooling profiles generated with interactive radiation compared to static or fixed cooling profiles have profound effects on the convective diagnostics; this will be discussed in more detail in sections 4 and 5. The dashed red lines in figure 3b,c,e,f are interactive cooling profiles from simulations that are initiated with dry tropospheres; these are results from the multiple equilibria simulations described in sections 2.4 and 4.3.

These cooling profiles are very different from those obtained in *Anber et al.* [2015], who considered the effect of wind shear and static versus interactive radiation on convection in WTG simulations. In their figure 2, the radiative cooling profiles show a cooling of about 1 K day^{-1} from the surface to about 12 km only for weak surface fluxes; stronger surface fluxes generate cooling patterns reminiscent of stratiform clouds with strong cooling (-8 to -12 K day^{-1}) at about 12 km with strong warming (5-7 K day^{-1}) at an approximate cloud base of 8 km. Radiative cooling is negligible below 7 km in these cases. Somewhat similar cooling profiles (at least in the vicinity of the tropopause) are reported for disturbed regions in idealized RCE simulations [*Posselt et al.*, 2008; *Stephens et al.*, 2008]. In contrast, figure 3 shows cooling throughout the troposphere with magnitudes ranging from 1-4 K day^{-1} in convecting environments; the strongest cooling–about 5 K day^{-1}–occurs at the top of the boundary layer in domains with suppressed convection. Although not in perfect agreement, these cooling profiles reproduce gross features of what is observed in nature [*McFarlane et al.*, 2007]. Convecting profiles also agree with domain mean cooling profiles in the idealized RCE simulations [*Stephens et al.*, 2008], while the dry cooling profiles resemble those from the undisturbed regions in idealized RCE simulations [*Posselt et al.*, 2008].

2.4. Multiple equilibria

The pursuit of multiple equilibria in limited domain WTG simulations represents one strategy for investigating convective organization that occurs on larger scales. If the organization is characterized by strong moisture gradients in which regions of intensely precipitating convection is surrounded by regions of strong descent exhibiting a troposphere depleted of moisture, then multiple equlibria represents either the region of strong convection or the region of strong descent. We hypothesize that parameters or mechanisms which support multiple equilibria in WTG simulations are indicative of conditions that promote convective organization.

In order to investigate multiple equilibria, we perform parallel numerical experiments: in one set the tropospheric moisture is initialized with the RCE mixing ratio profile; in the other set, the intial tropospheric moisture is set to zero everywhere. All other boundary and prescribed forcing conditions are identical. Multiple equilibria exist if the initially moist troposphere sustains precipitating convection while the initially dry simulation remains dry with descent in the free troposphere. If the initially dry simulation develops precipitating convection, or if the initially moist simulation dries and exhibits descent in the steady state, then a single equilibrium exists. Varying model parameters so that we can identify circumstances which either support or suppress multiple equilibria can provide insight to mechanisms that are important for convective organization.

In this paper, we focus on the role of the thermodynamic environment and radiation treatment on convective organization. *Sessions et al.* [2015] performed a limited number of multiple equilibria experiments in different thermodynamic environments. In that work, the authors considered multiple equilibria in more stable and more moist environments (with perturbations identical to those in figure 2b,c,f), as well as in an environment with unperturbed thermodynamic profiles (i.e., figures 1 and 2e). Using static radiation (with the radiative cooling profile set by the RCE cooling profile), the authors considered how different parameterizations of horizontal moisture advection affected the existence of multiple equilibria. They found that their model–the same one used in this study–only supported multiple equilibria in an unperturbed environment and only when horizontal moisture advection was parameterized using lateral entrainment. In this work, we restrict our moisture treatment to lateral entrainment, and we permit radiation to cool interactively.

For this set of experiments, we restrict our radiation treatment to the static and interactive cases (as we will show in section 4, there is minimal difference in the characteristics of convection between the static and fixed profiles, so we don't perform multiple equilibria experiments with fixed radiative cooling). We also only consider environments which are less likely to support the dry equilibrium: more moist and/or more stable (corresponding to RCE perturbations shown in figure 2b,c,f). We repeat initially dry and moist simulations using wind speeds ranging from 3-10 m s^{-1} to identify a range of parameters which support multiple equilibria, and to compare how that range changes with radiation treatment in different thermodynamic environments.

3. Diagnosing convection

In addition to determining the conditions which permit multiple equilibria, it is useful to diagnose the characteristics of convection in different thermodynamic environments. *Sessions et al.* [2015] identified a set of diagnostics that not only served to quantify the characteristics of convection, but also elucidated the relationships between the convective environment and the precipitation produced by the convection. We will use the same diagnostics for this work, and they are described below.

The primary diagnostic used to characterize convection is the space and time averaged precipitation rate. To zeroth order, it indicates conditions which permit or suppress convection, and provides a measure of the strength of convection when the precipitation rate is non-zero. By itself, however, precipitation rate is a limited diagnostic since different vertical and horizontal distributions of convective updrafts may produce similar precipitation rates. Consequently, we also calculate the saturation fraction, an instability index, a measure of deep convective inhibition, and the normalized gross moist stability. These are all defined below. It is also useful to consider vertical profiles of potential temperature and mixing ratio anomalies, as well as vertical profiles of mass flux. The mass flux is calculated as the product of the density and total vertical velocity. In WTG simulations, the total velocity is the sum of resolved and WTG velocity fields. In taking the domain average, the contribution from the resolved velocity is zero since what goes up must come down. Consequently, the only non-zero contribution to the mass flux is from the WTG vertical velocity:

$$\text{mass flux} = \rho w_{wtg} \quad . \tag{8}$$

The saturation fraction provides a measure of the moisture contained in the model domain. It is the vertically integrated precipitable water divided by the vertically integrated saturated precipitable water. As in *Sessions et al.* [2015], we approximate it as

$$S = \frac{\int \rho(s - s_d)dz}{\int \rho(s^* - s_d)dz} \tag{9}$$

where the vertical integrals are taken over the entire depth of the model (20 km deep). $s_d = c_p \ln(\theta/T_R)$ is the dry entropy ($c_p = 1005$ J kg^{-1}K^{-1} is the specific heat at constant pressure, and $T_R = 300$ K is a constant reference temperature), s is the moist entropy (with θ replaced by θ_e in the dry entropy definition), and s^* is the saturated moist entropy.

Perturbations applied to the reference potential temperature profiles change the atmospheric stability. We quantify this by an instability index, Δs^* [*Raymond et al.*, 2011; *Gjorgjievska and Raymond*, 2014; *Sessions et al.*, 2015], defined as

$$\Delta s^* = s^*_{low} - s^*_{high} \quad , \tag{10}$$

where s^*_{low} is the domain mean saturated moist entropy in the level between 1 and 3 km, and s^*_{high} is the domain mean saturated moist entropy in the level between 5 and 7 km. At a given altitude, s^* is nearly a function of temperature only, thus the difference in the mean s^* at two levels gives a measure of the atmospheric stability that often co-varies with negative lower tropospheric convective available potential energy (CAPE). Smaller values of Δs^* correspond to more stable environments; larger values are more unstable.

Deep convective inhibition (DCIN) expresses the likelihood that low-level parcels will reach their respective levels of free convection [*Raymond et al.*, 2003]. It is defined as

$$\mathrm{DCIN} = s_t^* - s_b, \tag{11}$$

where s_t^* is the threshold entropy for convection given by the average of the saturated moist entropy in the layer between 1750 and 2000 m; s_b is the boundary layer moist entropy, averaged from the surface to 1750 m. Small or negative values of DCIN are conducive to developing deep convection; large values inhibit it.

Finally, we also calculate the normalized gross moist stability (NGMS). First introduced by *Neelin and Held* [1987], the gross moist stability provides a measure of the response of convection to the large-scale forcing. It is defined as the export of some quantity that is approximately conserved in moist processes (usually moist static energy or moist entropy) divided by a measure of the strength of the convection [see the review by *Raymond et al.*, 2009]. We define NGMS, Γ, as the export of moist entropy divided by the lateral import of moisture:

$$\Gamma = \frac{T_R[\nabla_h \cdot (\rho s \mathbf{v})]}{-L[\nabla_h \cdot (\rho r_t \mathbf{v})]} = \frac{T_r \int \nabla_h \cdot (\rho s \mathbf{v}) dz}{-L \int \nabla_h \cdot (\rho r_t \mathbf{v}) dz}. \tag{12}$$

The square brackets signify a vertical integral over the troposphere and ∇_h is the horizontal divergence operator. $T_R = 300$ K is a reference temperature, and $L = 2.833 \times 10^6$ J kg^{-1} is the sum of the latent heats of condensation and freezing; these constants are included to non-dimensionalize Γ. The temperature profile of the reference environment has a strong influence on the shape of the vertical mass flux profile [*Raymond and Sessions*, 2007;

Gjorgjievska and Raymond, 2014; *Sessions et al.*, 2015]; this in turn controls the lateral entrainment and detrainment of moisture and moist entropy (denominator and numerator in equation 12, respectively), and thus controls the magnitude of the precipitation rate. In the steady state, the numerator in equation 12 is equal to the net entropy forcing ($F_S - R$, where F_S is the surface moist entropy flux due to surface heat and moisture fluxes, and R is the vertically integrated entropy sink per unit mass due to radiation); while the denominator is equal to the net precipitation ($P - E$, where P is the precipitation rate and E is the evaporation). Together, the steady state NGMS is inversely related to the net precipitation:

$$\Gamma = \frac{T_R(F_S - R)}{L(P - E)} \quad , \tag{13}$$

[*Raymond et al.*, 2007]. For most experiments, the SST is held constant and the surface wind speed is relaxed to a constant value over a timescale of a few hours so that F_S is approximately constant; if radiation is not interactive, then R is also constant and $P - E \propto 1/\Gamma$ so that the net precipitation is entirely controlled by NGMS (which is indirectly controlled by the vertical mass flux). Permitting radiation to cool interactively may adjust R, though we still expect a strong correlation between the net precipitation and the inverse NGMS.

4. Results

The diagnostic quantities in this work are either given as vertical profiles or scalar variables. In all cases, the computational domain is horizontally averaged, and a time average is taken over the last two weeks of the one month segment of the simulation that represents a specific thermodynamic environment. Because a single numerical simulation runs for 90 days with a perturbation added in 30 day intervals, the last hour of the 30 day increment is excluded in the time average to avoid including conditions representative of the newly perturbed environment. *Sessions et al.* [2015] showed time series of precipitation rate for all combinations of perturbations used in that study; their figures 6-8 are identical to the static radiation experiments in this paper so we refer to that work for details regarding the time dependence (there are no significant differences, so we consider only the time mean quantities). However, we do point out a caveat from that work that holds here: in most cases, two weeks in sufficient for the model to equilibrate following a perturbation applied to the reference profiles. However, if horizontal moisture advection is parameterized by lateral entrainment (as it is in this work), then perturbing the reference θ toward a less stable environment results in a gradual decrease in free tropospheric moisture. The reason for this is that lateral entrainment only permits environmental moisture to enter the domain, no removal of moisture occurs at detraining levels (see the second term in equation 5); thus, the only mechanism for the removal of moisture from the model domain is radiative subsidence down the moisture gradient. This relatively slow process means that the model may not quite be in a statistically steady state during the 2 week period for which the time averages are taken. However, as in *Sessions et al.* [2015], the difference between the almost-steady state and the true steady state values are small compared to the differences between different thermodynamic enviroments, so we analyze the diagnostics as they are, keeping this caveat in mind. Although the time-dependent results in *Sessions et al.* [2015] were shown for static radiation, interactive radiation shows similar behavior (not shown) and thus the discussion holds for all the simulations which become less stable (all other perturbations adjust quickly).

4.1. Vertical profiles

In order to determine the extent to which the model domain adopts the thermodynamic conditions of the reference environment, we display the potential temperature and mixing ratio anomalies for each reference environment (figures 4 and 5). The imposed perturbations are shown with thin black lines; different colors correspond to different radiative cooling treatments. Note that throughout the free troposphere (from the top of the boundary layer at 1 km to the 15 km tropopause) the model-derived θ anomalies are nearly identical to the imposed anomalies; this is an expected consequence of enforcing the WTG approximation. The only significant difference in the model's θ anomalies from the imposed occur when the environment is both more moist and more stable (figure 4c). In this case the model is warmer in a layer between 1 and 9 km; this is likely a consequence of the latent heating due to the strong convection in this layer (compare with the vertical mass flux in figure 6).

We would also like to point out that more stable environments (figure 4a-c) have very cool boundary layers while less stable environments (figure 4g-i) have relatively warmer boundary layers. This was also demonstrated in *Sessions et al.* [2015]; in fact, the blue lines corresponding to static radiation in this paper are identical to the blue lines in that paper (in both papers, blue lines represent simulations with static radiation and laterally entrained moisture). There is negligible difference in θ anomalies between fixed and static radiation, though we see that the boundary layer is cooler when interactive radiation is used in less stable environments compared to fixed or static cooling profiles (cf., figure 4g-i).

In contrast, the mixing ratio anomalies in figure 5 show a much greater range of variability compared to the imposed reference anomalies. Note that the horizontal axes are different in figure 5: panels a-f range from -2 to 2 g kg^{-1}, panels g-i range from -10 to 4 g kg^{-1} (all tick marks are in 2 g kg^{-1} intervals). There are three important observations regarding the domain mean moisture in different environments with different radiation treatments:

1. moisture anomalies are more influenced by θ perturbations than r_t perturbations,

2. less stable environments severely dry the troposphere,

3. there are no obvious significant differences between radiation treatments, except interactive radiation more thoroughly evacuates domain moisture in less stable environments (5g-i) than do static or fixed radiation. It turns out that this is more important than we would guess.

The first two observations are consistent with the results from *Sessions et al.* [2015]. In more stable environments (figure 5a-c), there are positive moisture anomalies in the free troposphere, even in drier environments (figure 5a). The depth and magnitude of the positive moisture anomalies increase when more moisture is available from the environment. Less stable environments (figure 5g-i) exhibit extremely negative moisture anomalies, even in moister environments. When radiative cooling is interactive, there is drying through an even deeper layer; the boundary layer is not as moist (non-interactive radiation, on the contrary, shows a 2 g kg^{-1} positive moisture anomaly in the boundary layer), and the 1 km layer just above the boundary layer is devoid of moisture.

With respect to differences in radiation treatments, we note that in most cases, moisture anomalies are very similar with two exceptions:

1. as discussed above, there is more drying in less stable environments when radiation cools interactively.

2. There is almost no difference in the non-interactive cooling profiles (static versus fixed), except in a drier environment with an unperturbed reference θ profile (figure 5d).

The second exception is seen in figure 5d. In this case, the interactive radiative cooling profile produces moisture anomalies very similar to those produced with the static cooling profile; a fixed cooling profile, on the other hand, produces a larger dry anomaly at 3 km and almost no drying in the 1 km layer just above the boundary layer. The latter effect results from the shallow convection evident in the fixed radiation case (see figure 6d).

Vertical mass flux profiles are shown in figure 6. As in the moisture anomalies shown in figure 5 and in *Sessions et al.* [2015], we note that the shape of each mass flux profile is primarily governed by the atmospheric stability, with weaker influences by atmospheric moisture and radiation treatment. More stable environments generate more "bottom-heavy" convective profiles, while less stable environments suppress convection altogether. These results are discussed in detail in *Sessions et al.* [2015]; here we focus on the effects of radiation.

There is very little difference between interactive and static mass flux profiles in more stable environments (compare red and blue lines in figure 6a-c) despite differences in radiative cooling profiles (figure 3a-c) where interactive radiation exhibits stronger cooling in the upper troposphere and weaker cooling in the lower troposphere compared to the static cooling profile. In contrast, the biggest difference between static and fixed radiative cooling profiles is seen in a more stable environment (compare blue and black lines in figures 3 and 6a-c). When there is uniform radiative cooling below 12 km (fixed at -1.8 K day^{-1}), the vertical mass flux is weaker compared to imposing the RCE cooling profile. Independent of radiation treatment, the strength of the vertical mass flux in a more stable environment with bottom heavy convection is quite sensitive to the environmental moisture profile; more moist environments have much stronger updrafts, with domain mean maxima ranging from 0.08 to nearly 0.1 kg m^{-2}s^{-1} (all horizontal tick marks denote increments of 0.02 kg m^{-2}s^{-1}), while drier environments produce maxima of only 0.01-0.02 kg m^{-2}s^{-1}.

If the atmospheric stability is unperturbed (figure 6d-f), then the environmental moisture represented by the reference r_t profile governs the strength of convection. In this case, drier environments produce weak vertical motion through the troposphere (it is very weak when the cooling rate is fixed), while there is upward motion in the upper troposphere and descent in the lower troposphere if the reference moisture profile is unperturbed or moister (figure 6e,f). This case also shows a distinction between radiation treatments: the radiative cooling profiles are nearly identical for static and interactive radiation (see figure 3d-f), and the mass flux profiles are similar. The fixed cooling profile obviously differs (it is not as cool above 5 km, but it is cooler below; see figure 3), as does the level of convergence according to the mass flux profiles. Positive mass flux indicates upward motion while negative value indicate descent; by mass continuity, there will be convergence wherever mass flux is increasing with altitude. It is interesting to note that the level that separates upward motion from descent (within the layer of convergence) for the static and interactive radiative cooling profile occurs at about 3 km; it is located at 5 km when fixed radiative cooling is prescribed. Since the convergence affects the lateral entrainment of moisture and moist entropy (for example, see equation 5), this is likely to affect the convection and the corresponding diagnostics. We discuss this in the next subsection.

Finally, we compare the radiation treatments in less stable environments. In this case, there is little difference between the static and fixed cooling profiles; they both exhibit descent throughout the free troposphere and weak upward motion in the boundary layer. In contrast, interactive radiation generates descent all the way to the surface. Although the weak circulation produced when radiation is non-interactive may seem insignificant, this has profound consequences with respect to mechanisms responsible for organizing convection.

One more thing to point out in the context of the mass flux profiles are the dashed lines in figure 6b,c,e,f. These correspond to mass flux profiles which were initiated with zero tropospheric moisture (the multiple equilibria simulations). These will be discussed in more detail in section 4.3.

4.2. Diagnostic Relationships

In order to better understand how convection responds to changes in the environment–and how interactive radiation affects that response–it is useful to consider the relationships between the diagnostic quantities which characterize the convection. The precipitation rate provides a meaningful measure for the strength of convection. In figure 7, we show scatter plots of precipitation rate as a function of saturation fraction, instability index, NGMS, and DCIN (all defined in section 3). The symbols correspond to the reference environments (figures 1 and 2), and the colors correspond to different radiation treatments.

As expected, the precipitation rate varies strongly with the domain mean saturation fraction; this agrees qualitatively with observations [*Bretherton et al.*, 2004; *Peters and*

Neelin, 2006; *Raymond et al.*, 2009; *Masunaga*, 2012] and modeling studies [*Raymond et al.*, 2007, 2015; *Daleu et al.*, 2015b]. The results also agree with *Sessions et al.* [2015]: more stable environments (indicated by upright triangles) exhibit higher saturation fractions and stronger precipitation rates, especially in moister environments, while less stable environments (denoted by inverted triangles) suppress deep convection and produce extremely low saturation fraction values with zero precipitation rates. This holds for all radiation options. *Sessions et al.* [2015] showed that the extremely low saturation fractions in less stable environments were observed only when horizontal moisture advection was parameterized via lateral entrainment of moisture (as is done in this study); it is a result of radiatively driven subsidence down the moisture gradient with no sources of moisture to offset the drying. Thus, the only source of moisture in the entire column is a result of surface evaporation which moistens the boundary layer. Note that when radiative cooling is interactive (red colors in figure 7), the saturation fraction is even smaller. This is because the radiatively-driven subsidence extends all the way to the surface: the vertical mass flux shows descent in the boundary layer only with interactive radiation (see red profiles in figure 6g-i). This is a consequence of the extreme cooling at the top of the boundary layer (figure 3g-i) which results in less moistening in the boundary layer (figure 5g-i) compared to non-interactive radiative cooling profiles. It appears that differences in radiation treatments are most significant in situations which suppress deep convection.

The instability index quantifies the atmospheric stability. Figure 7b shows that lower values of the instability index result in higher precipitation rates; higher values completely inhibit precipitating convection. The lines shown connect conditions having the same reference moisture perturbations (i.e. solid lines connect experiments with different perturbations applied to the potential temperature, but the moisture profile remains unperturbed; dashed and dotted lines have moist anomalies, $r_{RCE} + \delta r_t$, or dry anomalies, $r_{RCE} - \delta r_t$). The main observations to note are

1. the strong dependence of precipitation rate on instability index, and
2. the sensitivity of precipitation rate on the environmental moisture with a given instability index.

The latter observation is most apparent for a low instability index (corresponding to a more stable environment); moister environments (filled upright triangles) exhibit much higher precipitation rates than unperturbed (half-filled triangles) or drier (empty triangles) environments.

The NGMS is a diagnostic that measures the convective response to changes in the large-scale forcing. In the steady state, it is inversely proportional to the net precipitation (see equation 13). Figure 7c shows the relationship between the precipitation rate and the steady state NGMS. The inversely proportional relationship is immediately apparent with large values of precipitation rates occuring for small, positive values of NGMS. There are a few caveats to this figure, however. The first is that this relationship holds for constant surface fluxes and radiative cooling (i.e., numerator in equation 13). While the surface fluxes are the same for all of the experiments shown (the surface wind speeds and SSTs are the same), we might expect that the vertically integrated radiative cooling may result in slight differences for different radiation treatments. This is not observed because, despite the different radiative cooling profiles in convecting environments, the vertically integrated net cooling is approximately the same. The fixed cooling rate (-1.8 K day^{-1}) is explicity chosen to have a value that matches the vertically integrated value of the static profile. We have less control over the vertical integral of the interactive radiative cooling profile; however, it is nearly identical to the static profile if the reference potential temperature profile is unperturbed (figure 3d-f), and the excess cooling aloft in more stable environments seems to be offset by the reduced cooling in the lower troposphere. In other words, despite the differences in the radiative cooling profiles for the radiation treatments in environments which support convection, the vertically integrated radiative source of entropy remains approximately constant ($R \approx$ constant in equation 13). Another caveat is that NGMS is not always a particularly useful diagnostic. Recall that NGMS is defined as the ratio of moist entropy export to moisture import. In RCE conditions–or in thermodynamic environments which are close to RCE conditions–there is no net import or export of either of these quantities and NGMS is undefined (zero divided by zero). This can result is very large fluctuations in the instantaneous quantities and we obtain very little diagnostic value in these situations. This is evident by examining the bulls-eyes (representing unperturbed reference environments) in figure 7c; the values of NGMS range from about 0.5 to 2.7; this reflects large fluctuations corresponding to rapid transitions between import and export of the moisture and moist entropy as convection evolves. Nevertheless, in conditions which have a definite tendency for either import or export of moisture and moist entropy, NGMS can be very useful for diagnosing convection.

There is one more important observation to make regarding the NGMS in these simulations: that is the behavior of NGMS in non-precipitating environments. These occur in less stable environments and are clearly identified by the inverted triangles along the zero precipitation line in figure 7c. In non-precipitating cases, the NGMS can be either small or negative [*Sessions et al.*, 2010, 2015]. Negative values imply that both moisture and moist entropy are simultaneously exported from the domain. In all non-precipitating cases, moisture is exported from the domain, so whether NGMS is positive or negative depends on whether moist entropy is imported or exported. Moist entropy is only exported if radiation is interactive: interactive radiation induces strong radiative subsidence which extends through the boundary layer all the way to the surface (see the mass flux profiles in figure 6g-i). In contrast, if radiation is not interactive, weak ascent in the boundary layer (black and blue lines in figure 6g-i) permits weak import of moist entropy which results in positive NGMS. This is an extremely important result: in self-aggregation studies, the dry subsiding regions in an RCE domain which exhibited convective self aggregation had negative gross moist stability which served as a positive feedback that enforced the aggregation [*Bretherton et al.*, 2005]. With perhaps one exception [*Tompkins*, 2001b], convective organization has thus far only been demonstrated in 3-dimensional RCE domains with interactive radiation [*Tompkins and Craig*, 1998; *Bretherton et al.*, 2005; *Muller and Held*, 2012; *Wing and Emanuel*, 2013; *Wing and Cronin*, 2015]. This suggests that interactive radiation more readily promotes organization by extending the free tropospheric descent through the boundary layer, thus enforcing conditions which suppress the development of new convection in these subsiding regions, while enforcing the export of moisture and moist entropy to the aggregated regions that sustain strong deep convection.

Finally, we examine the diagnostic, DCIN. The results are similar to those presented in *Sessions et al.* [2015]: small or negative values of DCIN are conducive to developing deep convection and occur with non-zero precipitation rates in figure 7d. Larger values of DCIN, mostly associated with less stable environments (inverted triangles), correspond to conditions which suppress deep convection and thus have zero precipitation. As discussed in *Sessions et al.* [2015], the conditions most conducive for strong precipitation–more stable and more moist (filled upright triangles)–have negative DCIN values that are close to zero. The novel result in this study is the extremely large values of DCIN which occur in unstable environments with interactive radiation (red inverted triangles in figure 7d). DCIN is defined in terms of a threshold entropy (s_t^*, equation 11) and the boundary layer entropy. The threshold entropy, being an average of the saturated moist entropy, depends only on the temperature which is effectively fixed by the enforcement of WTG. The boundary layer moist entropy, on the other hand, is a measure of the moisture in the lowest 1.75 km layer. As we've discussed, permitting radiation to cool interactively drives the subsidence all the way to the surface and effectively evacuates the moisture from the domain, with the exception of trace amounts due to evaporation at the surface. This results in a very small s_b, and consequently very large DCIN. This situation is especially hostile to developing new convection, and thus reinforces the organization of convection on the large-scale.

In addition to identifying how each of the diagnostics relate to precipitation rate, it is useful to consider how they relate to each other. Figure 8 shows the relationships between saturation fraction and instability index, saturation fraction and NGMS, NGMS and DCIN, and saturation fraction and DCIN. Again, these results very closely follow those reported in *Sessions et al.* [2015]:

1. There is a strong relationship between saturation fraction and instability index,

2. There is a strong relationship between saturation fraction and NGMS for high saturation fractions and small NGMS,

3. There is not much correlation between NGMS and DCIN, and

4. Little correlation exists between saturation fraction and DCIN, though DCIN is somewhat higher in less stable environments (inverted triangles, figure 8d).

The primary differences between the results in this work and *Sessions et al.* [2015] occur in a less stable environment with interactive radiation (red inverted triangles). These include:

1. extreme drying resulting in very low values of saturation fraction,

2. negative NGMS as a consequence of moist entropy export (rather than import when non-interactive radiation is used), and

3. extremely high values of DCIN suggesting particularly hostile environments for initiating new convection.

Sessions et al. [2015] compared the effects of different parameterizations of horizontal moisture advection. They found very little difference in the parameterizations when the domain supported precipitating convection; the biggest distinctions occured when the domain was not precipitating. For example, less stable environments exhibited much lower saturation fractions and higher DCIN values when moisture was laterally entrained (with static radiation) compared to other parameterizations of horizontal moisture advection. Figure 8 shows that this effect is amplified when radiation is interactive.

Although there doesn't appear to be a strong correlation between saturation fraction and NGMS, if we consider only NGMS ¡ 1 (which represent good diagnostic values), then there is an inverse relationship in which smaller values of NGMS correspond to higher saturation fractions (see inset of figure 8b).

Finally, we note that there is no obvious relationship between NGMS and DCIN (figure 8c). As discussed in *Sessions et al.* [2015], we do not expect a strong relationship between these two diagnostics based on the simple analytic theory of *Raymond and Fuchs* [2007]. They posited that different types of convective disturbances were destabilized by different mechanisms; for example, convectively-coupled Kelvin waves are destabilized by convective inhibition, whereas moisture mode disturbances (such as the Madden-Julian Oscillation) are destabilized by NGMS. The real atmosphere likely has a combination of these mechanisms contributing to the wide variety of convective disturbances. The point here, however, is that we do not expect a correlation between NGMS and DCIN since they represent different mechanisms for destabilizing convection. Nevertheless, it is interesting to note that the extremely high values of DCIN are related to conditions which exhibit negative gross moist stability; this is likely no accident since the descent in the boundary layer is responsible for both of these observations.

4.3. Multiple Equilibria

Multiple equilibria occur in conditions that permit both a persistent precipitating state, and one in which the free troposphere remains dry with no precipitation. The particular state that is realized depends on the initial tropospheric moisture [*Sobel et al.*, 2007; *Sessions et al.*, 2010; *Emanuel et al.*, 2013; *Daleu et al.*, 2015a]: initially dry tropospheres remain dry while initially moist tropospheres support the continuous development and decay cycle of active convection. The initial moisture profile, however, must exceed some minimum threshold in order to maintain convection [*Sessions et al.*, 2010; *Emanuel et al.*, 2013].

In this study, we investigate the existence of multiple equilibria in different thermodynamic environments using either static or interactive radiation. Since multiple equilibria in WTG simulations are hypothesized to be a proxy for self-aggregation in larger-domain

RCE simulations, understanding multiple equilibria in this context will help identify (or verify) mechanisms important to convective organization.

For this part of the study, we consider only a subset of our thermodynamic environments:

1. unperturbed RCE profiles (figure 2e),
2. more stable environments (figure 2b),
3. moister environments (figure 2f), and
4. moister, more stable environments (figure 2c).

The reason for only performing a subset of these is that less stable environments do not support precipitation with initially moist profiles, thus, it is extremely unlikely that convection will spontaneously develop when the troposphere is initially dry. Since we are interested in the robustness of multiple equilibria under conditions which support strong convection, we also exclude drier environments.

In the previous sections, we found that the most significant differences in radiation treatment was between interactive and non-interactive radiative cooling; no significant qualitative differences occured as a result of the shape of the cooling profile if radiation was non-interactive. Thus, we also restrict this part of the investigation to a comparison between the interactive and static radiation treatments.

In order to determine how robust multiple equilibria are for different environments and different radiation treatments, we performed parallel experiments–with one set initialized with the RCE or perturbed moisture profile, and one set intially dry–for wind speeds ranging from 3-10 m s^{-1}. This includes a value smaller than that used to calculate the RCE state (5 m s^{-1}), and thus is expected to sustain a single, non-precipitating steady state (at least with unperturbed reference profiles); and larger values which are more likely to support a single precipitating steady state in unperturbed conditions.

Figure 9 shows results of the multiple equlibria experiments for static and interactive radiation for the subset of thermodynamic environments explored. The solid lines indicate simulations which were initialized with the reference moisture profile; dashed lines connect experiments which were initially dry. It is clear that both the environment and radiation treatment affect the existence of multiple equilibria. This is very interesting considering the results of *Sessions et al.* [2015]: they found that multiple equilibria only existed with a surface wind speed of 7 m s^{-1} when horizontal moisture advection was parameterized using lateral entrainment (all experiments in that work used static radiation). Those results are included within the blue lines in figure 9c; in this work we have included a larger range of surface wind speeds (both greater than and less than 7 m s^{-1}) in order to facilitate a comparison with interactive radiation.

Across this range of wind speeds, experiments using static radiation exhibit interesting behavior in different environments compared to those using interactive radiation. In particular, when a static radiative cooling profile is prescribed, figure 9a,b show that a more stable environment supports precipitating convection even if the troposphere is initially dry. Only a single equilibrium exists in this case (solid and dashed blue lines), even at wind speeds that are weaker than that of the RCE simulation (5 m s^{-1}). It is interesting to note, however, that multiple equilibria exists for static radiation simulations with unperturbed θ profiles (blue lines in figure 9c,d). In these cases, the range of multiple equilibria is affected by the reference moisture environment, with a moister environment exhibiting multiple equilibria only when the RCE wind speed is used (see 5 m s^{-1} case in figure 9d). Multiple equilibria exist over a broader range when the environment is unperturbed (figure 9c).

Permitting radiation to interact with convection drastically changes the conditions under which the domain supports multiple equilibria: multiple equilibria exists over a range of wind speeds even in environments which are both moister and more stable (e.g., figure 9b). In unperturbed environments, interactive radiation supports multiple equilibria over the entire range of wind speeds shown in figure 9, although it is destroyed if wind speeds are increased to 15 m s^{-1} (not shown).

In addition to the conditions which permit multiple equilibria, is it instructive to compare the effect of interactive radiation in convecting environments. In particular, whether radiative cooling is static or interactive has very little influence on the precipitation rate. This is in contrast to the results from *Anber et al.* [2015], who found that interactive radiation significantly decreased precipitation rates relative to static cooling, especially at higher surface fluxes (which occur for higher wind speeds in this work). They attributed this to lower NGMS caused by import of air with low moist static energy at mid-levels; this in turn was a consequence of increased vertical motion at upper levels, reminiscent of stratiform precipitation. Though our model and the WTG implementation differs significantly from the Weather and Research Forecasting model used in *Anber et al.* [2015], we speculate that the most significant contribution to the different behavior is a consequence of the radiative cooling profiles generated by the two models (compare their figure 2 with figure 3 in this paper). Their cooling profiles exhibit strong ($\sim$ -10 K day^{-1}) cooling at 12 km with 5 K day^{-1} heating at 8 km. The heating is likely a result of trapping longwave radiation at stratiform base [see, eg., figure 1 in *Raymond and Zeng*, 2000]. The maximum

WTG vertical velocity occurs at 10 km–the approximate altitude that separates warming below this level from cooling above. This warming heats the upper troposphere (0.5-3.5 K) compared to their RCE profiles. In comparison with the results from the unsheared experiments using a prescribed fixed cooling rate of 1.5 K day^{-1} [*Anber et al.*, 2014], WTG vertical velocities were weaker than those using the static or interactive profiles, even with stronger surface fluxes. *Daleu et al.* [2015a] reported that variations in radiative cooling near the tropopause in several different models influenced the precipitation rate in RCE simulations; it is likely that this affect also influences WTG simulations.

To briefly summarize the important observations from figure 9, we note the following:

1. More stable environments only generate precipitating convection with static radiative cooling, even with weak surface fluxes compared to RCE conditions.

2. In contrast, interactive radiation supports multiple equilibria in a wide range of environments, including those with greater stability.

3. Whether radiation is static or interactive has little effect on the precipitation rate in convecting environments.

These observations have important consequences for understanding the interplay between the thermodynamic environment and radiation in convective organization. This will be discussed further in section 5.

In the mean time, it is useful to analyze the other diagnostic variables defined in section 3 in order to understand the difference between static and interactive radiation in the context of multiple equilibria simulations. Figure 10 shows scatter plots of precipitation versus saturation fraction, instability index, NGMS, and DCIN for static (left column) and interactive (right column) radiative cooling. The symbols correspond to numerical simulations in the different thermodynamic environments, while the colors correspond to the surface wind speed, v_y, imposed perpendicular to the 2-dimensional plane of the model. In some cases, multiple experiments were performed so there are several symbols that correspond to identical conditions. As these diagnostics are all plotted against precipitation rate, it is easy to distinguish the non-precipitating experiments from the precipitating ones. Although we include the simulations which were initialized with zero tropospheric moisture, we do not make a distinction between simulations with different moisture initialization profiles. Important differences between static and interactive radiation are indicated with gray shading.

In examining the difference between the static and interactive radiation diagnostics, a quick glance shows generally similar behavior in all simulations which support precipitation; the biggest differences occur in simulations with zero precipitation. For example, saturation fraction values for non-precipitating simulations with interactive radiation are much lower (< 0.4, figure 10b) compared to that for static radiation (< 0.6, figure 10a). As discussed before, this is a consequence of the strong radiative cooling at the top of the boundary layer (figure 3b,c,e,f) that drives descent all the way to the surface (figure 6b,c,e,f). The result is a much drier boundary layer and consequently smaller saturation fraction.

At first glance, there is little difference in the relationship between precipitation rate and instability index; upon closer inspection, however, we note that only the interactive radiation simulations have experiments with zero precipitation in more stable environments (compare upright triangles–smaller instability indices–in figure 10c,d). These reflect the multiple equilibria observed in figure 9a,b for interactive radiation only.

The panels illustrating the NGMS-precipitation relationship also yield a subtle, yet important difference between the effects of interactive and static radiation. For the precipitating states, NGMS qualitatively observes the inversely proportional relationship with precipitation rate (equation 13). Note that–in contrast to the different thermodynamic environments and radiation treatments seen in figure 7c–precipitating cases do not lie on a single curve. The greater surface fluxes of moist entropy (F_S in equation 13) associated with greater wind speeds produce higher precipitation rates for a given value of NGMS. This is similar to the results shown in *Sessions et al.* [2010]. However, NGMS exhibits the most significant differences between radiation treatments for the non-precipitating simulations: static radiation produces NGMS values which are all positive, and which range from slightly greater than zero to about 1.75. In contrast, NGMS takes much smaller values and even becomes negative when radiation is interactive. Given the distribution of gross moist stability in RCE self-aggregation studies–which show positive values in the convecting regions and negative values in the dry regions [*Bretherton et al.*, 2005]–this may be a significant result. We discuss this in more depth in the next section.

The most drastic difference between static and interactive radiation is observed in the values of DCIN when the domain is devoid of convection. When static radiation is used, DCIN is negative in the simulations which exhibit zero precipitation (figure 10g), suggesting that despite the dry steady state, convection would be easy to trigger in these experiments. In stark contrast are the values of DCIN when the domain is not precipitating but radiation is cooling interactively. In this case, DCIN lies between the considerably greater values of 20 and 60 J kg^{-1}K^{-1}, suggesting a situation which would require a very significant perturbation to trigger convection in these conditions. Note that the highest values correspond to the lowest surface wind speeds; increasing the surface wind speed increases the surface fluxes of moisture and moist entropy which increases the boundary layer moist entropy (s_b in equation 11) and gradually decreases DCIN. As mentioned previously (but not shown), multiple equilibria do not exist with interactive radiation and a surface wind speed of 15 m s^{-1} (DCIN in this case is about 2 J kg^{-1}K^{-1} for an unperturbed environment); it may be that a critical DCIN marks the conditions which separate the precipitating states from those which severely inhibit convection. If we consider multiple equilibria–or more generally dry WTG domains–as a proxy for the descending regions associated with large-scale convective organization, then radiation appears to strongly support existing organization by prohibiting the development of convection in the dry regions via strong inhibition. We will discuss this in more detail in the next section.

To highlight the most important results regarding multiple equilibria in different thermodynamic environments with either static or interactive radiative cooling, we note:

1. Interactive radiation permits multiple equilibria even in more stable and moister evironments which do not support a dry equilibrium state when radiation is static.

2. When radiation interactively cools a dry troposphere, convection is strongly suppressed as a consequence of radiatively driven subsidence that extends through the boundary layer to the surface; this results in

(i) lower saturation fractions,

(ii) negative NGMS, and

(iii) extremely high DCIN

compared to simulations where a static radiative cooling profile is employed.

In the next section, we discuss how these observations fit within our current understanding of convective organization.

5. Discussion

We now discuss our results in the context of what we understand so far about the mechanisms responsible for organization in models. As in previous work that analyzes multiple equilibria using the WTG approximation [*Sobel et al.*, 2007; *Sessions et al.*, 2010; *Emanuel et al.*, 2013; *Sessions et al.*, 2015], we assume the dry and moist equilibria in WTG simulations are analogous to dry, subsiding regimes and moist, precipitating convective regimes, respectively, in larger domain RCE simulations. We begin with a brief summary of some of the studies which analyze convective organization in cloud system resolving models (CRMs).

Held et al. [1993] is perhaps one of the earliest to report convective organization in RCE simulations. Using a 2-dimensional domain with interactive radiation, they found that convection organized into bands of propagating convection which oscillated from westward to eastward. In an attempt to remove this oscillation, they relaxed the mean zonal winds to zero; in this case, the initially randomly distributed convection evolved to a stationary region of convection. Imposing modest windshear destroyed all forms of organization in this model. They attributed the convective organization to a memory in the moisture field rather than to the low-level convergence pattern. These experiments were performed with surface temperatures of 25° and 30°C; the former experiments took longer to organize, exhbited slightly different character, and exhibited a smaller albedo than the experiments over a warmer surface. The character of convective organization as a function of surface temperature has been echoed in more recent studies [*Khairoutdinov and Emanuel*, 2010; *Posselt et al.*, 2012; *Wing and Emanuel*, 2013; *Wing and Cronin*, 2015].

Tompkins and Craig [1998] performed some of the earliest 3-dimensional RCE simulations which exhibited convective organization. Organization took the form of moist and dry bands of convection in a (100 km)^2 domain. Both interactive surface fluxes and interactive radiation were necessary for organization to develop; horizontally homogenizing either of these fields destroyed the convective organization. This was also shown to be the case in *Bretherton et al.* [2005], which is perhaps the earliest reported example of convection corralled into a single, circular stationary region by virtue of the appearance of an incipient dry spot with a subsiding troposphere that expands until all convection is confined to a single region.

Most examples of convective organization using a 3-dimensional CRM have reported that interactive radiation is an essential mechanism for convection to organize [*Tompkins and Craig*, 1998; *Bretherton et al.*, 2005; *Stephens et al.*, 2008; *Muller and Held*, 2012; *Wing and Emanuel*, 2013]. A notable exception is *Tompkins* [2001b], who demonstrated convective organization on a domain with rectangular "channel" geometry with a horizontally homogeneous, fixed radiative cooling rate. In that work, the convection organized into bands of precipitation separated by dry subsiding regions which migrated either East or West. Though the organization is not as extreme as in simulations of self-aggregation demonstrated in *Bretherton et al.* [2005]; *Muller and Held* [2012]; *Wing and Emanuel* [2013], (perhaps quantifable by the aggregation index introduced by *Tobin et al.* [2012]), it is certainly organized with distinct dry and moist regions. In a recent study of convective aggregation using channel geometry, *Wing and Cronin* [2015] used the same model that was originally used to study self-aggregation that manifested as a single, stationary circular patch [*Bretherton et al.*, 2005; *Muller and Held*, 2012; *Wing and Emanuel*, 2013]. They found that changing the geometry of the domain reorganized the convection from a single, stationary circular region to a banded structure, similar to that found in *Tompkins* [2001b]. To evaluate mechanisms responsible for organization, *Wing and Cronin* [2015] decomposed the frozen moist static energy budget to examine the dominant feedbacks with channel geometries over SSTs ranging from 280-310 K. At an SST of 300 K–the same as that used in *Tompkins* [2001b]–they found that while both shortwave and longwave radiation were positive feedbacks in the early stages of organization, surface fluxes exhibited a stronger positive feedback. *Tompkins* [2001b] attributed organization to positive feedbacks between convection and water vapor. In another study of RCE using channel geometry, *Stephens et al.* [2008] investigated radiative convective feedbacks in 2- and 3-dimensional simulations with interactive and static radiative cooling. Simulations with interactive radiation showed obvious signatures of organization, which they attributed to radiative heating gradients induced by the existence of high clouds produced in moist convecting regions, and the absence of high clouds in dry regions. It is interesting to note that although organization is strong when interactive radiation is invoked, there is evidence for weak organization when radiation is homogenized [see figure 3c in *Stephens et al.*, 2008], similar to *Tompkins* [2001b]. However, the organization does not persist with longer model integration.

Bretherton et al. [2005] reported radiative cooling as a positive feedback which transported moist static energy (MSE) from the driest columns to the moistest columns. Because temperature gradients are weak, most of the energy transport is associated with moisture transport from dry regions to moist regions, thus reinforcing the aggregated state. This transport is a result of strong radiative cooling near the top of the boundary layer which drives subsidence and, by mass continuity, results in export from the lowest 1 km of the dry regions. The export of MSE from the dry regions corresponds to negative gross moist stability there. In more recent work, *Muller and Held* [2012] and *Wing and Emanuel* [2013] specifically investigated the roles of longwave and shortwave radiation as well as surface fluxes. Both of these studies report that longwave radiation is the dominant positive feedback for the aggregated state. *Muller and Held* [2012] verified the role of longwave cooling in the upgradient transport of MSE by suppressing the longwave cooling from liquid condensates below 1 km; this effectively suppressed self-aggregation. A similar removal of longwave cooling above 2 km or a homogenization of shortwave radiation still permitted aggregation. This is in direct agreement with *Bretherton et al.* [2005]. Similarly, *Wing and Emanuel* [2013] performed a decomposition of contributions to the frozen moist static energy (FMSE) budget; they found that while shortwave radiation played an important role in the initial destabilization of the RCE state to aggregation, longwave radiation was the dominant positive feedback in maintaining the aggregated state. This decompositon also highlighted the role of convergence of FMSE into the moist regions, in agreement with *Bretherton et al.* [2005] and *Muller and Held* [2012]. Similarly, in an investigation of the role of cold pools in aggregation, *Jeevanjee and Romps* [2013] reported that dry patches exhibited a dry, deep circulation and a shallow, moist circulation, both of which reinforced convective organization, in agreement with the above studies.

The results presented in this paper are not only consistent with the analogous simulations of self-aggregation, but they help to elucidate the role of interactive radiation in convective organization. Furthermore, they provide evidence that while interactive radiation strongly enhances organization, it is not a requirement for its existence, which is consistent with the fact that *Tompkins* [2001b] demonstrated organized convection with homogeneous, fixed radiative cooling. To see this, consider the major results of this paper in the context of spontaneously organized convection in large, 3-dimensional RCE simulations:

1. **The dry state exhibits strong cooling at the top of boundary layer only with interactive radiation** (see figure 3g-i and dry equilibria states in 3b,c,e,f). This was also reported in the dry regions of larger self-aggregated simulations [*Bretherton et al.*, 2005; *Muller and Held*, 2012].

2. **The boundary layer in the dry state is slightly cooler** (figure 4g-i) **and drier** (figure 5g-i) **when interactive radiation is invoked compared to prescribing a static profile.** The cooling is likely a consequence of the strong radiative cooling in this layer (figure 3). The drying is a consequence of subsidence; *Jeevanjee and Romps* [2013] reported a drier boundary layer in dry regions in their investigation of the role of cold pools in organizing convection.

3. **The strong cooling at the top of the boundary layer in the dry state when interactive radiation is used results in strong descent near the top of the boundary layer which entrains environmental air in this layer; this descends to the surface where it drives net export of moist entropy (or analogously, MSE).** This is identical to the circulation described in *Bretherton et al.* [2005]; *Muller and Held* [2012]; *Jeevanjee and Romps* [2013], which results in upgradient transport of MSE, and consequently negative gross moist stability in the dry region. In contrast,

prescribing a static radiative cooling profile does not permit the strong cooling at the top of the boundary layer, which changes the boundary layer circulation entirely. In the latter case, environmental air is imported at the surface and exported at the top of the boundary layer (figure 6g-i, black and blue lines). Moist entropy (or equivalently MSE) is transported down gradient and NGMS is positive.

4. **The boundary layer circulation–where descent in the boundary layer results in net export of moist entropy–maintains a dry equilibrium state even in conditions which support strong convection** (see, e.g., figure 9b). Interactive radiation effectively expands the range of parameter space which permits multiple equilibria and, by analogy, presumably also convective organization. Most RCE simulations report that interactive radiation is required for convective organization; *Tompkins* [2001b] is a notable exception.

5. **Multiple equilibria exists even in the absence of interactive radiation; this would suggest that convection can organize with fixed, homogeneous radiative forcing** (see figure 9c). Although our WTG simulations with static radiation exhibit multiple equilibria in a very restricted parameter space compared to interactive radiation, multiple equilibria exist without interactive radiation (although it does not with alternate parameterizations of the large-scale, including the damped gravity wave approximation, *Daleu et al.* [2015a], and a spectral version of WTG, *Herman and Raymond* [2014]). This suggests that while interactive radiation makes it much easier to drive convection to an organized state, it is not essential. *Bretherton et al.* [2005] presented a simple model which predicted that an RCE simulation would aggregate if the sum of fitting parameters corresponding to surface-flux feedbacks and radiative feedbacks were greater than some

critical value. In this simple model, it would be possible for aggregation to occur with homogeneous static radiative cooling if the surface-flux feedbacks were sufficiently strong. As mentioned above, *Tompkins* [2001b] demonstrated convective organization with fixed, homogeneous radiative cooling; while the organization is not as strong as exhibited in models with interactive radiation, it organizes nevertheless. *Stephens et al.* [2008] also provides evidence of weak (albeit temporary) organization in idealized RCE simulations with fixed radiation.

If it is possible to organize convection without radiative-convective feedbacks, what other mechanisms could be responsible for the organization? In the one example we have which exhibits organization in the absence of interactive radiation, *Tompkins* [2001b] attributes organization to strong feedbacks between convection and water vapor. This explanation is consistent with the "moisture memory" proposed by *Held et al.* [1993].

Recently, *Craig and Mack* [2013] presented a coarsening model for self-organization of tropical convection. The main requirement for organization is that convection in RCE can be modeled as a bistable system where drying overcomes moistening for small saturation fractions, but moistening dominates at larger saturation fractions. This requirement is supported by an earlier equilibrium study of RCE in a two-column model [*Nilsson and Emanuel*, 1999] as well as in studies of multiple equilibrium and self-aggregation. *Craig and Mack* [2013] argue that radiative cooling determines the spatial mean–but not the spatial distribution–of precipitation. Instead, the location of convection is governed by lower tropospheric moisture content (though interactive radiation may enhance moisture inhomogeneities and thus be favorable to organization). They and others [e.g. *Emanuel et al.*, 2013] argued that organization is most likely a result of a combination of radiative-convective interactions, water vapor-convection interactions, and surface fluxes. According to our results as well as others, it is possible to eliminate at least one of these for convection to exhibit at least weak organization. For example, *Muller and Held* [2012] were able to obtain self-aggregation with homogeneous surface flux forcing; thus, despite the fact that homogenizing surface fluxes of moisture inhibits sharp moisture gradients that characterize the organization, radiation and water vapor interactions with convection were sufficient to permit organization.

The requirement for interactive radiation likely depends on model and model parameters. For example, *Wing and Cronin* [2015] found that the contributions of clouds to the radiative feedbacks were sensitive to the radiation scheme invoked. *Wing and Emanuel* [2013] showed that shortwave radiation was responsible for destabilizing the domain to an organized state, while longwave radiation was the dominant mechanism responsible for maintaining the organized state. In comparison, our multiple equilibria simulations start with the analogous organized state (one dry domain and one moist); running the simulation determines whether those represent statistically steady states. We do not consider how the destabilization occurs in the first place, and it may be possible that interactive radiation is necessary for that, though the results from *Tompkins* [2001b] [and to a lesser degree, *Stephens et al.*, 2008] suggest otherwise. It is interesting to note that the examples which organize convection in the absence of interactive radiation use rectangular domains; perhaps the broken symmetry of the geometry–which changes the character of convection in RCE simulations even with interactive radiation [*Wing and Cronin*, 2015]–plays a role in the organization. Several studies have speculated that this is a consequence of the dominance of the second-mode gravity waves in initiating convection in two dimensions [e.g., *Mapes*, 2000; *Bretherton et al.*, 2005; *Stephens et al.*, 2008; *Fuchs et al.*, 2014, among others]. Furthermore, *Bretherton et al.* [2005] suggested that isotropic propagation of these gravity waves in square 3-dimensional geometries reduced the effectiveness of this instability mechanism. Thus other mechanisms, perhaps related to large-scale circulations, become important.

Convection can also organization as a consequence of imposed vertical wind shear, even with non-interactive radiation [*Robe and Emanuel*, 2001; *Cohen and Craig*, 2006]. Windshear can also inhibit convective organization, as *Held et al.* [1993] demonstrated in their 2-dimensional RCE model. Perhaps reducing the symmetry of the system—either by changing the geometry of the computational domain or dynamically by imposing vertical wind shear—invokes an alternate mechanism which permits organization in the absence of interactive radiation.

Dynamical asymmetries may also arise from changes in the rotational environment. Recently, *Raymond et al.* [2015] proposed a theory of tropical convection based on balanced dynamics. Observations and theories suggest that positive mid-tropospheric vorticity anomalies generate virtual temperature anomalies with cooling below and warming aloft (similar to the more stable perturbations shown in figure 2a,b,c). As shown previously [*Raymond and Sessions*, 2007; *Gjorgjievska and Raymond*, 2014; *Sessions et al.*, 2015] and in this work, the more stable environment promotes more "bottom-heavy" convection which laterally entrains more moist low-level air and thus increases the precipitation rate. Similarly, a negative vorticity anomaly would generate the opposite temperature dipole anomaly which we have demonstrated can strongly suppress convection. Thus, subtle changes in the thermodynamic environment which may be induced by dynamic variations in vorticity significantly contribute to convective organization. Our results both here and in *Sessions et al.* [2015] suggest that is an important organization mechanism even in the absence of interactive radiation; however, interactive radiation strongly reinforces the organization.

On a somewhat related note, *Davis* [2015] investigated the process of spontaneous organization in a rotating RCE domain. His objective was to understand the origin of rotating coherent structures preceding tropical cyclogenesis. As in previous studies which invoked rotation on an RCE domain [*Bretherton et al.*, 2005; *Nolan et al.*, 2007], convection aggregated in the presence of interactive radiation. *Davis* [2015] also performed simulations with radiation calculated from Newtonian relaxation which was effectively a homogenization of the radiative cooling. Although convective aggregation was prevented in this case, the model generated moist and dry patches. Presumably, these patches could not grow in this environment without a mechanism to transport moisture upgradient. *Davis* [2015] showed that interactive radiation generated a balanced secondary circulation as a consequence of the gradient in radiative cooling between moist and dry regions (this circulation was absent when radiative cooling was homogenized). Profiles of relative vorticity within moist patches exhibited positive anomalies at 6 km whether or not radiation was interactive; however, the anomalies were much stronger with interactive radiation. It is interesting to note that in contrast to RCE simulations of self-aggregation in symmetric geometries without rotation [i.e. *Bretherton et al.*, 2005; *Muller and Held*, 2012; *Wing and Emanuel*, 2013], organization in this experiment does not initiate with the growth of an incipient dry spot. Instead, dry regions appear simultaneously with moist regions, and moist regions (associated with positive potential vorticity anomalies) merge during the organization process. Evidently, rotation changes the process of convective organization compared to simulations without rotation; perhaps rotation can be considered a type of dynamical asymmetry.

Given our results in the context of previous studies, we hypothesize that

1. Interactive radiation is not necessary for maintaining organization in models (although this may only be true in systems with reduced geometric or dynamic symmetry).

2. However, interactive radiation drastically increases the parameter space which permits a model to exhibit organization.

It is interesting that the boundary layer circulations in the dry state in this work–and the implications for upscale transport of moist entropy and thus negative gross moist stability–are in agreement with the observations made for the large-scale RCE simulations which exhibit convective organization. However, it is also interesting to consider some of the other convective diagnostics in this work. The extremely low saturation fraction and zero precipitation rate are in easy agreement with the dry regions of organized convection. A less obvious connection, however, can be made when we consider the behavior of DCIN in our model. *Tompkins* [2001b] calculated the more conventional quantity, convective inhibition (CIN), in several regions in the organized state. In the dry region, he reported high values of CIN compared to convecting regions or even dry regions which are embedded in a convective envelope. In this work, we found that interactive radiation has a profound effect on DCIN when radiation cools interactively compared to when it does not (see figure 7g-h). As discussed previously, interactive radiation permits the extreme drying just above and in the boundary layer which results in a nearly negligible boundary layer moist entropy and a correspondingly large DCIN. In developing stochastic and mesoscopic models for tropical convection, *Majda and Khouider* [2001] proposed CIN as an order parameter for identifying the existence of multiple radiative-convective equilibria. Considering that self-aggregation in a large-domain RCE simulation initiates organization as the growth of a single dry spot [*Bretherton et al.*, 2005; *Muller and Held*, 2012; *Wing and Emanuel*, 2013], perhaps DCIN (or CIN) represents an important parameter for diagnosing the dry regimes in convective organization. Indeed, it may be fruitful to consider a separate theory for the relationships between convective (or non-convective) diagnostics for dry regimes separately from moist regions which sustain convection. Clearly a relationship between precipitation and other diagnostics has limited use if precipitation is zero. However, we present evidence that other diagnostic quantities, NGMS and DCIN specifically, exhibit different characteristics in the convecting regimes compared to the non-convecting regimes. It may prove to be quite informative to analyze these relationships in models and observational datasets in non-precipitating conditions to determine if there are any systematic tendencies which determine conditions favorable for organization. This, in turn, could be used to incorporate organization in convective parameterizations, as suggested by *Mapes and Neale* [2011] and *Tobin et al.* [2012].

6. Summary

Using a cloud system resolving model with the large scale parameterized by the weak temperature gradient (WTG) approximation, we have investigated the role of radiation in organizing deep tropical convection. Convective organization in larger domain simulations of radiative-convective equilibrium (RCE) is characterized by regions of strong, precipitating convection with adjacent dry regions of descent.

We characterize convective organization in our limited domain simulations by the ability of the model to suppress convection in the domain. This can either occur as a consequence of the thermodynamic environment, or in situations which support multiple equilibria–either a precipitating or a dry steady state–depending on the initial moisture profile. The underlying goal of this work is to examine how interactive radiation influences convective organization by examining several diagnostics–including vertical profiles of radiative cooling and mass flux, and steady state values of precipitation, saturation fraction, instability index, normalized gross moist stability, and deep convective inhibition–both in simulations which exhibit active convection and those which suppress it.

Radiative cooling in this investigation is either interacting or non-interacting. Interactive radiative cooling calculates the cooling rate based on the water vapor content in the model domain. The non-interactive radiative cooling profile is either calculated as the time and domain mean cooling profile from an RCE simulation, or is prescribed to be a fixed -1.8 K day^{-1} through most of the free troposphere (the rate is chosen as the vertical average of the static cooling profile).

Thermodynamic environments supporting precipitating convection–represented by either unperturbed RCE or more stable reference profiles–show very little difference in the characteristics of convection when radiative cooling is interactive compared to when it is not. In contrast, the biggest differences in radiation treatments occur in dry, non-precipitating environments (which are either less stable, or which are represented by the dry equilibrium in conditions which support multiple equilibria). In a subsiding atmosphere, radiative cooling is strong above the boundary layer; this induces a boundary-layer circulation which imports moist entropy at the top of the boundary layer, but exports higher values of moist entropy near the surface, resulting in a net export of moist entropy (or analogously, moist static energy). This up-gradient transport of moist entropy results in a negative gross moist stability, and it is analogous to the circulations induced in larger simulations of radiative convective equilibrium (RCE) in which convection exhibits spontaneous organization [referred to as self-aggregation, e.g., *Bretherton et al.*, 2005; *Muller and Held*, 2012; *Wing and Emanuel*, 2013]. As a consequence of this circulation, saturation fractions are excessively diminished and deep convective inhibition is strongly enhanced in the presence of interactive radiation, independent of thermodynamic environment, as long as convection is suppressed. It is interesting that negative gross moist stability only occurs in the steady state when radiation cools interactively.

In this work, we also explored the effect of interactive radiation on the model's ability to exhibit multiple equilibria. We found that interactive radiation not only permitted multiple equilibria over a larger range of surface wind speeds, but it also permitted the existence of multiple equilibria in conditions which otherwise favor strong convection (more stable and more moist). In contrast, static radiative cooling in more stable environments always produced precipitation, even when surface wind speeds were reduced compared to RCE values (where we would expect radiative cooling to dominate convection).

While interactive radiation strongly enhances conditions which support convective organization, the existence of dry steady states–either in multiple equilibria or as a consequence of thermodynamic environments which are unfavorable to convection–suggests that interactive radiation is not absolutely essential for convective organization. Indeed, as others have suggested, several mechanims are at play–radiative-convective feedbacks, precipitation-moisture feedbacks, horizontal moisture advection, and vertical wind shear–

and organization is most easily achieved when some combination of these act in concert. However our results here, along with some previous work, suggest that not all have to be in effect, including what seems to be the dominant facilitator in convective organization: interactions between radiation and convection (or clear sky). However, in absence of radiative interactions, other mechanisms may require either a geometric or dynamic asymmetry to destabilize the convective domain to organization.

Acknowledgments. We'd like to thank Chimene Daleu, David Raymond, Saska Gjorgjievska, Greg Bothun, and George Craig for helpful discussions. This work was supported by U. S. National Science Foundation Grants AGS-1056254, ATM-1021049, and AGS-1342001. The model used to generate the data is available at http://kestrel.nmt.edu/∼raymond/tools.html. Scripts and model parameters used in this paper are available upon request from the corresponding author; please send requests via email to sessions@kestrel.nmt.edu.

References

Anber, U., S. Wang, and A. Sobel (2014), Response of atmospheric convection to vertical wind shear: Cloud-system-resolving simulations with parameterized large-scale circulation. part i: Specified radiative cooling, *J. Atmos. Sci.*, *71*, 2976–2993, doi:10.1175/JAS-D-13-0320.1.

Anber, U., S. Wang, and A. Sobel (2015), Effect of surface fluxes versus radiative cooling on tropical deep convection, *J. Atmos. Sci.*, submitted.

Back, L. E., and C. S. Bretherton (2009), On the relationship between SST gradients, boundary layer winds, and convergence over the tropical oceans, *J. Climate*, *22*, 4182–

4196, doi:10.1175/2009JCLI2392.1.

Bretherton, C. S., and P. K. Smolarkiewicz (1989), Gravity waves, compensating subsidence and detrainment around cumulus clouds, *J. Atmos. Sci.*, *46*, 740–759.

Bretherton, C. S., T. Uttal, C. W. Fairall, S. E. Yuter, R. A. Weller, D. Baumgardner, K. Comstock, R. Wood, and G. B. Raga (2004), The EPIC 2001 stratocumulus study, *Bull. Am. Meteor. Soc.*, *85*, 967–977.

Bretherton, C. S., P. N. Blossey, and M. Khairoutdivnov (2005), An energy-balance analysis of deep convective self-aggregation above uniform SST, *J. Atmos. Sci.*, *62*, 4273–4292.

Cohen, B. G., and G. C. Craig (2006), Fluctuations in an equilibrium convective ensemble. Part II: Numerical experiments, *J. Atmos. Sci.*, *63*, 2005–2015.

Craig, G. C., and J. M. Mack (2013), A coarsening model for self-organization of tropical convection, *J. Geophys. Res.*, *118*, 1–9, doi:10.1002/jgrd.50674.

Daleu, C. L., S. J. Woolnough, and R. S. Plant (2012), Cloud-resolving model simulations with one- and two-way couplings via the weak temperature gradient approximation, *J. Atmos. Sci.*, *69*, 3683–3699, doi:10.1175/JAS-D-12-058.1.

Daleu, C. L., R. S. Plant, S. J. Woolnough, S. Sessions, M. J. Herman, A. Sobel, S. Wang, D. Kim, A. Cheng, G. Bellon, P. Peyrille, F. Ferry, P. Siebesma, and L. van Ulft (2015a), Intercomparison of methods of coupling between convection and large-scale circulation: I. Comparison over uniform surface conditions, *J. Adv. Model. Earth Syst.*, doi:10.1002/2015MS000468.

Daleu, C. L., R. S. Plant, S. J. Woolnough, S. Sessions, M. J. Herman, A. Sobel, S. Wang, D. Kim, A. Cheng, G. Bellon, P. Peyrille, F. Ferry, P. Siebesma, and L. van Ulft (2015b), Intercomparison of methods of coupling between convection and large-scale circulation: II. Comparison over non-uniform surface conditions, *J. of Adv. Model. Earth Syst.*

Davis, C. A. (2015), The formation of moist vortices and tropical cyclones in idealized simulations, *J. Atmos. Sci.*, *72*, 3499–3516, doi:10.1175/JAS-D-15-0027.1.

Emanuel, K., A. A. Wing, and E. M. Vincent (2013), Radiative-convective instability, *J. Adv. Model. Earth Syst.*, *5*, doi:10.1002/2013MS000270.

Feng, Z., S. Hagos, A. K. Rowe, C. D. Burleyson, M. N. Martini, and S. P. de Szoeke (2015), Mechanisms of convective cloud organization by cold pools over tropical warm ocean during the AMIE/DYNAMO field campaign, *J. Adv. Model. Earth Syst.*, *7*, doi: 10.1002/2014MS000384.

Frank, W. M., and P. E. Roundy (2006), The role of tropical waves in tropical cyclogenesis, *Mon. Wea. Rev.*, *134*, 2397–2417.

Fuchs, Ž., S. L. Sessions, and D. Raymond (2014), Mechanisms controlling the onset of simulated convectively coupled Kelvin waves, *Tellus A*, *66*, 22107, doi: 10.3402/tellusa.v66.22107.

Gjorgjievska, S., and D. J. Raymond (2014), Interaction between dynamics and thermodynamics during tropical cyclogenesis, *Atmos. Chem. Phys.*, *14*, 3065–3082, doi: 10.5194/acp-14-3065-2014.

Held, I. M., R. S. Hemler, and V. Ramaswamy (1993), Radiative-convective equilibrium with explicit two-dimensional moist convection, *J. Atmos. Sci.*, *50*, 3909–3927.

Herman, M. J., and D. J. Raymond (2014), Wtg cloud modeling with spectral decomposition of heating, *J. Adv. Model. Earth Syst.*, *06*, doi:10.1002/2014MS000359.

Jeevanjee, N., and D. M. Romps (2013), Convective self-aggregation, cold pools, and domain size, *Geophys. Res. Lett.*, *40*, 1–5, doi:10.1002/grl.50204.

Khairoutdinov, M., and K. Emanuel (2013), Rotating radiative-convective equilibrium simulated by a cloud-resolving model, *J. Adv. Model. Earth Syst.*, *5*, 816–825, doi: 10.1002/2013MS000253.

Khairoutdinov, M. F., and K. Emanuel (2010), Aggregated convection and the regulation of tropical climate, paper presented at the 29th Conference on Hurricanes and Tropical Meterology, Am. Meteor. Soc., Tucson, Ariz.

Kiladis, G. N., M. C. Wheeler, P. T. Haertel, K. H. Straub, and P. E. Roundy (2009), Convectively coupled equatorial waves, *Reviews of Geophysics*, *47*(2), doi: 10.1029/2008RG000266, rG2003.

Lindzen, R. S., and S. Nigam (1987), On the role of sea surface temperature gradients in forcing low-level winds and convergence in the tropics, *J. Atmos. Sci.*, *44*, 2418–2436.

Majda, A. J., and B. Khouider (2001), Stochastic and mesoscopic models for tropical convection, *Proc. Natl. Acad. Sci.*, *99*, 1123–1128.

Mapes, B. (2000), Convective inhibition, subgrid-scale triggering energy, and stratiform instability in a toy tropical wave model, *J. Atmos. Sci.*, *57*, 1515–1535.

Mapes, B., and R. Neale (2011), Parameterizing convective organization to escape the entrainment dilemma, *J. Adv. Model. Earth Syst.*, *3*, doi:10.1029/2011MS000042.

Masunaga, H. (2012), Short-term versus climatological relationship between precipitation and tropospheric humidity, *J. Climate*, *25*, 7983–7990, doi:10.1175/JCLI-D-12-00037.1.

McFarlane, S. A., J. H. Mather, and T. P. Ackerman (2007), Analysis of tropical radiative heating profiles: A comparison of models and observations, *J. Geophys. Res.*, *112*, D14,218, doi:10.1029/2006JD008290.

Muller, C. J., and I. M. Held (2012), Detailed investigation of the self-aggregation of convection in cloud-resolving simulations, *J. Atmos. Sci.*, *69*, 2551–2565, doi:10.1175/JAS-D-11-0257.1.

Neelin, J. D., and I. M. Held (1987), Modeling tropical convergence based on the moist static energy budget, *Mon. Weat. Rev.*, *115*, 3–12.

Nilsson, J., and K. A. Emanuel (1999), Equilibrium atmospheres of a two-column radiative-convective model, *Q. J. R. Meteorol. Soc.*, *125*, 2239–2264, doi: 10.1002/qj.49712555814.

Nolan, D. S., E. D. Rappin, and K. A. Emanuel (2007), Tropical cyclogenesis sensitivity to environmental parameters in radiative-convective equilibrium, *Q. J. R. Meteorol. Soc.*, *133*, 2085–2107, doi:10.1002/qj.170.

Parodi, A., and K. Emanuel (2009), A theory for buoyancy and velocity scales in deep moist convection, *J. Atmos. Sci.*, *66*, 3449–3463, doi:10.1175/2009JAS3103.1.

Peters, O., and J. D. Neelin (2006), Critical phenomena in atmospheric precipitation, *Nat. Phys.*, *2*, 393–396, doi:10.1038/nphys314.

Polvani, L. M., and A. H. Sobel (2002), The Hadley circulation and the weak temperature gradient approximation, *J. Atmos. Sci.*, *59*, 1744–1752.

Posselt, D. J., S. C. van den Heever, and G. L. Stephens (2008), Trimodal cloudiness and tropical stable layers in simulations of radiative convective equilibrium, *Geophys. Res. Lett.*, *35*, L08,802, doi:10.1029/2007GL033029.

Posselt, D. J., S. C. van den Heever, G. L. Stephens, and M. R. Igel (2012), Changes in the interaction between tropical convection, radiation, and the large-scale circulation in a warming environment, *J. Climate*, *25*, 557-571, doi:10.1175/2011JCLI4167.1.

Raymond, D., . Fuchs, S. Gjorgjievska, and S. Sessions (2015), Balanced dynamics and convection in the tropical troposphere, *Journal of Advances in Modeling Earth Systems*, doi:10.1002/2015MS000467.

Raymond, D. J. (2001), A new model of the Madden-Julian Oscillation, *J. Atmos. Sci.*, *58*, 2807–2819.

Raymond, D. J., and Z. Fuchs (2007), Convectively coupled gravity and moisture modes in a simple atmospheric model, *Tellus*, *59A*, 627–640, doi:10.1111/j.1600-0870.2007.00268.x.

Raymond, D. J., and S. L. Sessions (2007), Evolution of convection during tropical cyclogenesis, *Geophys. Res. Lett.*, *34*, L06,811, doi:10.1029/2006GL028607.

Raymond, D. J., and X. Zeng (2000), Instability and large scale circulations in a two-column model of the tropical troposphere, *Quart. J. Roy. Meteor. Soc.*, *126*, 3117–3135.

Raymond, D. J., and X. Zeng (2005), Modelling tropical atmospheric convection in the context of the weak temperature gradient approximation, *Quart. J. Roy. Meteor. Soc.*, *131*, 1301–1320.

Raymond, D. J., G. B. Raga, C. S. Bretherton, J. Molinari, C. López-Carrillo, and Z. Fuchs (2003), Convective forcing in the intertropical convergence zone of the eastern Pacific, *J. Atmos. Sci.*, *60*, 2064–2082.

Raymond, D. J., S. L. Sessions, and Z. Fuchs (2007), A theory for the spinup of tropical depressions, *Q. J. Roy. Meteor. Soc.*, *133*, 1743–1754.

Raymond, D. J., S. L. Sessions, A. H. Sobel, and . Fuchs (2009), The mechanics of gross moist stability, *Journal of Advances in Modeling Earth Systems*, *1*(3), doi:

10.3894/JAMES.2009.1.9, 9.

Raymond, D. J., S. L. Sessions, and C. L. Carrillo (2011), Thermodynamics of tropical cyclogenesis in the northwest Pacific, *J. Geophys. Res.*, *116*, D18,101, doi: 10.1029:2011JD015624.

Robe, F. R., and K. A. Emanuel (2001), The effect of vertical wind shear on radiative-convective equilibrium states, *J. Atmos. Sci.*, *58*, 1427–1445.

Romps, D. M. (2012a), Weak pressure gradient approximation and its analytic solutions, *J. Atmos. Sci.*, *69*, 2835–2845, doi:10.1175/JAS-D-11-0336.1.

Romps, D. M. (2012b), Numerical tests of the weak pressure gradient approximation, *J. Atmos. Sci.*, *69*, 2846–2856, doi:10.1175/JAS-D-11-0337.1.

Sentic, S., S. L. Sessions, and Z. Fuchs (2015), Diagnosing convection with weak temperature gradient simulations of DYNAMO, *J. Adv. Model. Earth Syst.*, Accepted Author Manuscript, doi:10.1002/2015MS000531.

Sessions, S. L., S. Sugaya, D. J. Raymond, and A. H. Sobel (2010), Multiple equilibria in a cloud resolving model using the weak temperature gradient approximation, *J. Geophys. Res.*, *115*, D12110, doi:10.1029/2009JD013376.

Sessions, S. L., M. J. Herman, and S. Sentić (2015), Convective response to changes in the thermodynamic environment in idealized weak temperature gradient simulations, *J. Adv. Model. Earth Syst.*, *7*, 712–738, doi:10.1002/2015MS000446.

Sobel, A. H., and C. S. Bretherton (2000), Modeling tropical precipitation in a single column, *J. Climate*, *13*, 4378–4392.

Sobel, A. H., G. Bellon, and J. Bacmeister (2007), Multiple equilibria in a single-column model of the tropical atmosphere, *Geophys. Res. Lett.*, *34*, L22,804, doi:

10.1029/2007GL031320.

Stephens, G. L., S. van den Heever, and L. Pakula (2008), Radiative-convective feedbacks in idealized states of radiative-convective equilibrium, *J. Atmos. Sci.*, *65*, 3899–3916, doi:10.1175/2008JAS2524.1.

Su, H., C. S. Bretherton, and S. S. Chen (2000), Self-aggregation and large-scale control of tropical deep convection: A model study, *J. Atmos. Sci.*, *57*, 1797–1816.

Tobin, I., S. Bony, and R. Roca (2012), Observational evidence for relationships between the degree of aggregation of deep convection, water vapor, surface fluxes, and radiation, *J. Climate*, *25*, 6885–6903, doi:10.1175/JCLI-D-11-00258.1.

Tompkins, A. M. (2001a), On the relationship between tropical convection and sea surface temperature, *J. Climate*, *14*, 633–637.

Tompkins, A. M. (2001b), Organization of tropical convection in low vertical wind shears: The role of water vapor, *J. Atmos. Sci.*, *58*, 529–545.

Tompkins, A. M., and G. C. Craig (1998), Radiative-convective equilibrium in a three-dimensional cloud-ensemble model, *Q. J. R. Meteorol. Soc.*, *124*, 2073–2097.

Wang, S., and A. H. Sobel (2011), Response of convection to relative sea surface temperature: cloud-resolving simulations in two and three dimensions, *J. Geophys. Res.*, *116*, D11,119, doi:10.1029/2010JD015347.

Wang, S., and A. H. Sobel (2012), Impact of imposed drying on deep convection in a cloud-resolving model, *J. Geophys. Res.*, *117*, D02112, doi:10.1029/2011JD016847.

Wang, S., A. H. Sobel, and Z. Kuang (2013), Cloud-resolving simulation of TOGA-COARE using parameterized large scale dynamics, *J. Geophys. Res.*, *118*, 6290–6301, doi:10.1002/jgrd.50510.

Wing, A. A., and T. W. Cronin (2015), Self-aggregation of convection in long channel geometry, *Q. J. R. Meteorol. Soc.*, doi:10.1002/qj.2628.

Wing, A. A., and K. A. Emanuel (2013), Physical mechanisms controlling self-aggregation of convection in idealized numerical modeling simulations, *J. Adv. Mod. Earth Sys.*, *5*, 1–14, doi:10.1002/2013MS000269.

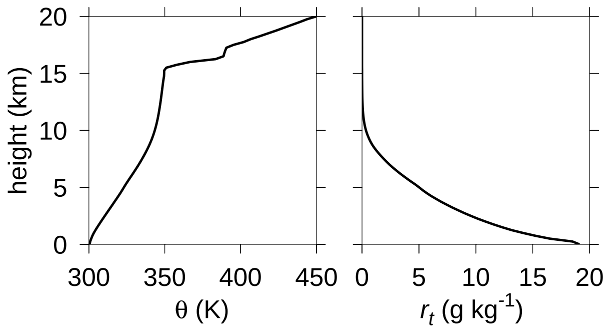

Figure 1. Radiative convective equilibrium (RCE) profiles of potential temperature (left) and total water mixing ratio (right) used as unperturbed reference profiles in WTG calculations. RCE is calculated over a uniform SST of 303 K, with surface wind speed of 5 ms^{-1} and interactive radiation on a 2D, 200 km horizontal domain. See text for more details. Reprinted with permission from *Sessions et al.* [2015].

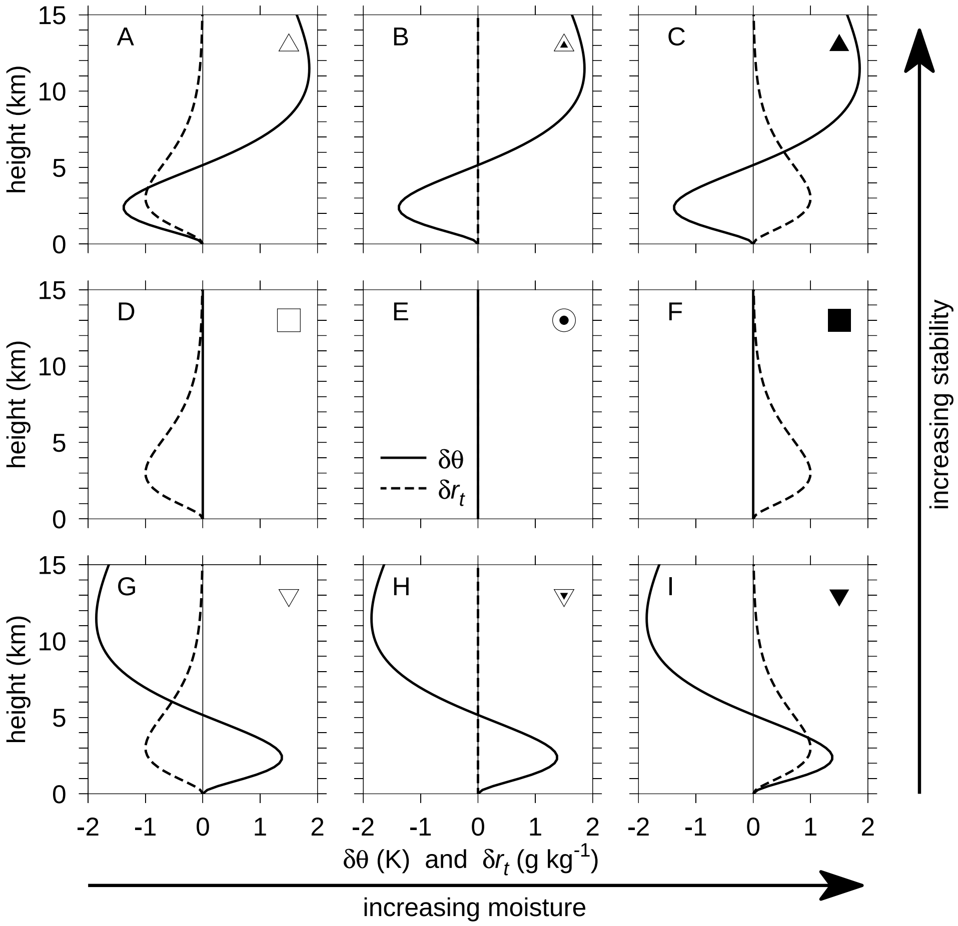

Figure 2. Perturbations added to the RCE reference profile. Solid lines represent perturbations to the potential temperature profiles, dotted lines give mixing ratio perturbations. The symbols in the upper right of each panel is a geometric representation of the thermodynamic environment where the shape corresponds to atmospheric stability and the shading corresponds to atmospheric moisture. Columns going from left to right have increasing moisture in the reference environment; in analogy with a glass of water, drier environments have empty symbols, unperturbed r_t profiles are half-filled, moister profiles are filled. Atmospheric stability increases from the bottom row to the top, and is represented by the geometric stability of the shape: more unstable environments have inverted triangles, unperturbed θ profiles have neutrally stable squares, more stable environments have uptright triangles. In order to easily distinguish when neither θ or r_t is perturbed (center panel), we use bulls-eyes. This figure serves as a legend for the results presented

Figure 2. (continued)

in section 4. It is reprinted with permission from *Sessions et al.* [2015].

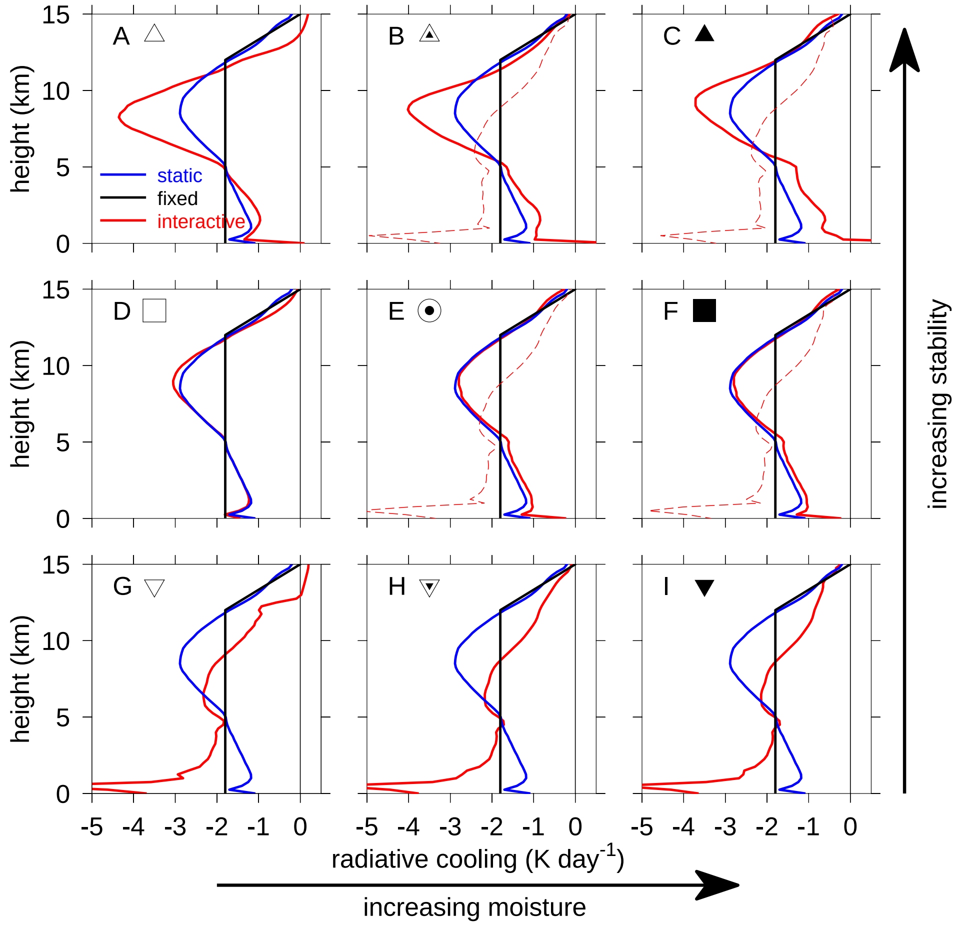

Figure 3. Radiative cooling profiles for each thermodynamic environment. Black and blue lines represent fixed (-1.8 K day^{-1}) and static (mean cooling profile from RCE simulation) cooling profiles. These are the same for all experiments. Red lines show the cooling profiles when radiation cools interactively. The thin dashed lines in (bcef) are cooling profiles in multiple equilibria runs where an initially dry troposphere remains dry. The symbols in the upper left corners are the geometric representation of the thermodynamic environments shown in figure 2.

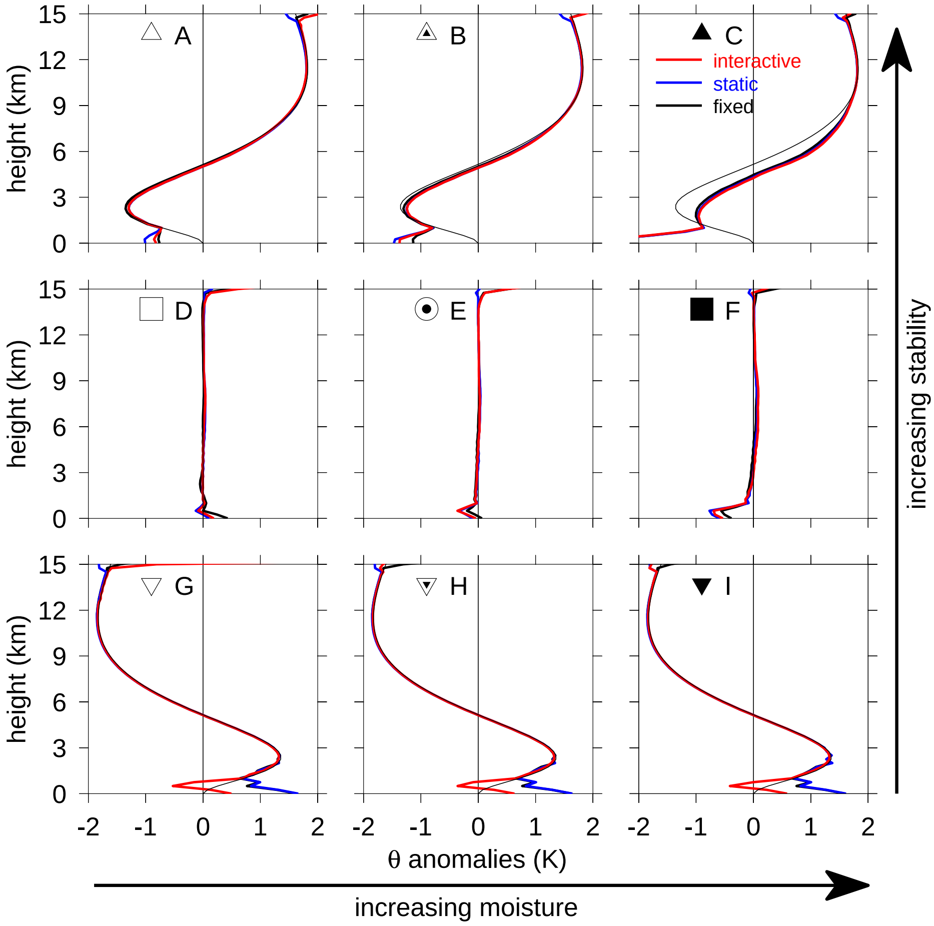

Figure 4. Potential temperature anomalies. The colors represent the different radiation treatments. The thin black line shows the potential temperature anomaly applied to the reference profile (same as the θ anomalies in figure 2).

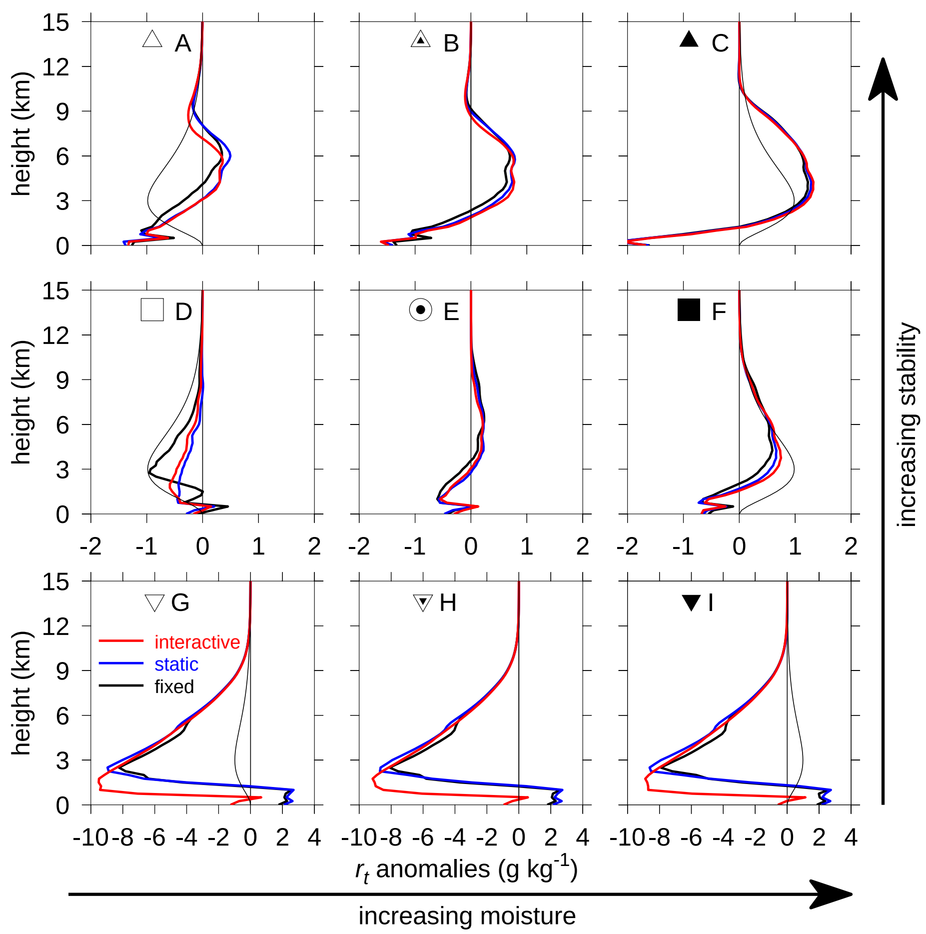

Figure 5. Total water mixing ratio anomalies. As in figure 4, the color represent the different radiation treatments. Note the different horizontal scale on the bottom row (g-i) compared to the top two rows (a-f). All horizontal tic marks represent increments of 2 g kg^{-1}.

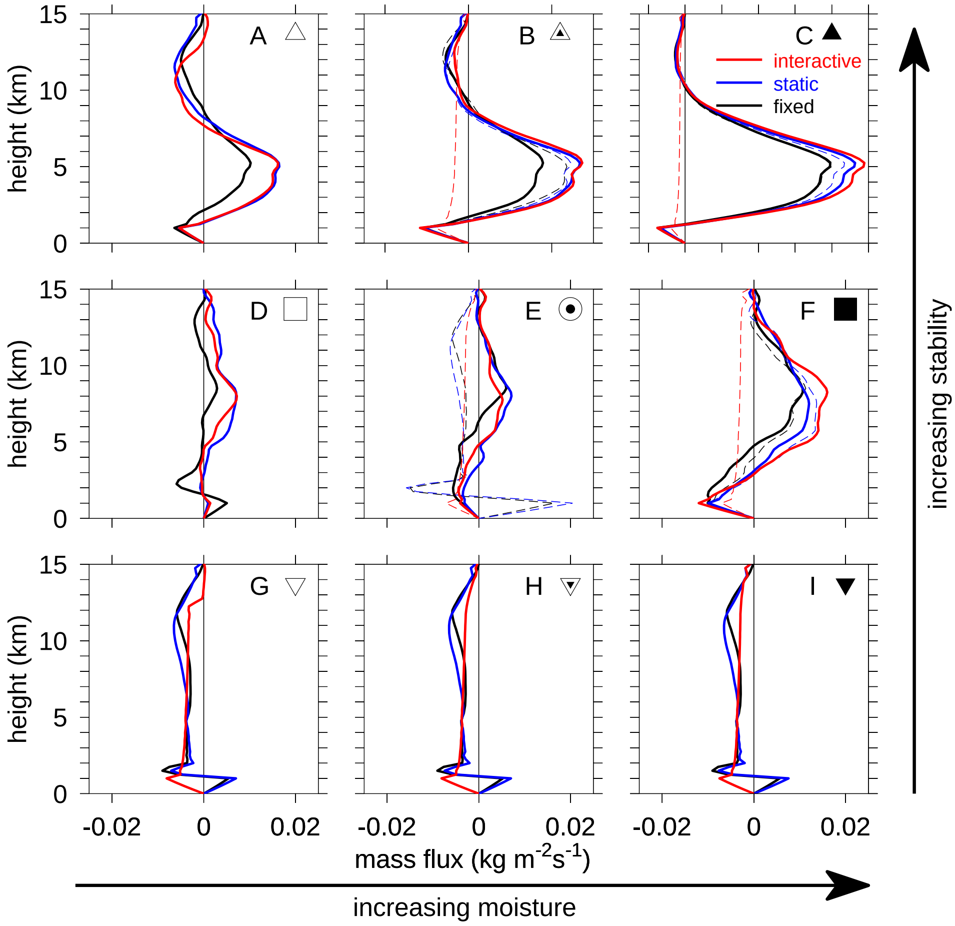

Figure 6. Mass flux profiles for different radiation treatments (distinguished by color) in different thermodynamic environments. Dashed lines show results when simulations are initiated with dry tropospheres (for multiple equilibria experiments, section 2.4). Note the different horizontal scales in the top row (a-c) compared to the bottom two rows (d-i). Tic marks represent 0.02 kg m^{-2}s^{-1} increments.

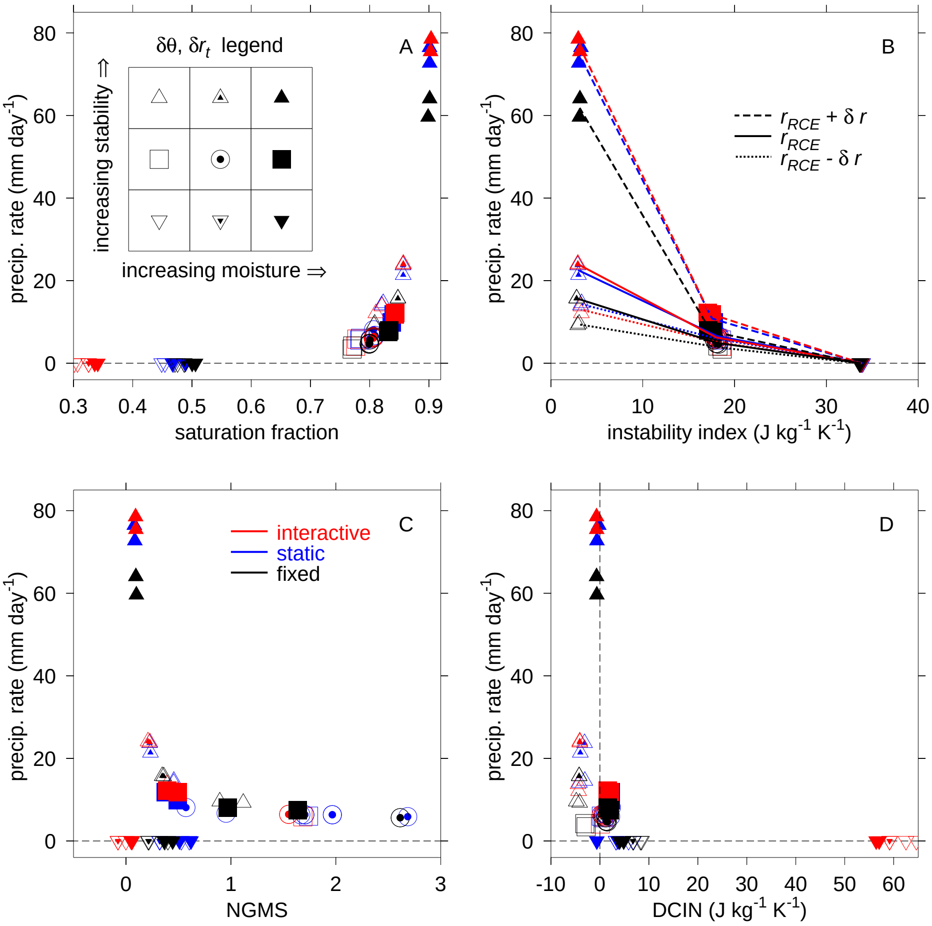

Figure 7. Precipitation rate as a function of (a) saturation fraction, (b) instability index, (c) NGMS, and (d) DCIN. Each symbol represents time and domain averages for simulations corresponding to different reference temperature and moisture profiles. The legend embedded in (a) corresponds to the perturbations shown in figure 2. The colors correspond to radiation treatment. The lines in (b) connect experiments with identical reference moisture profiles.

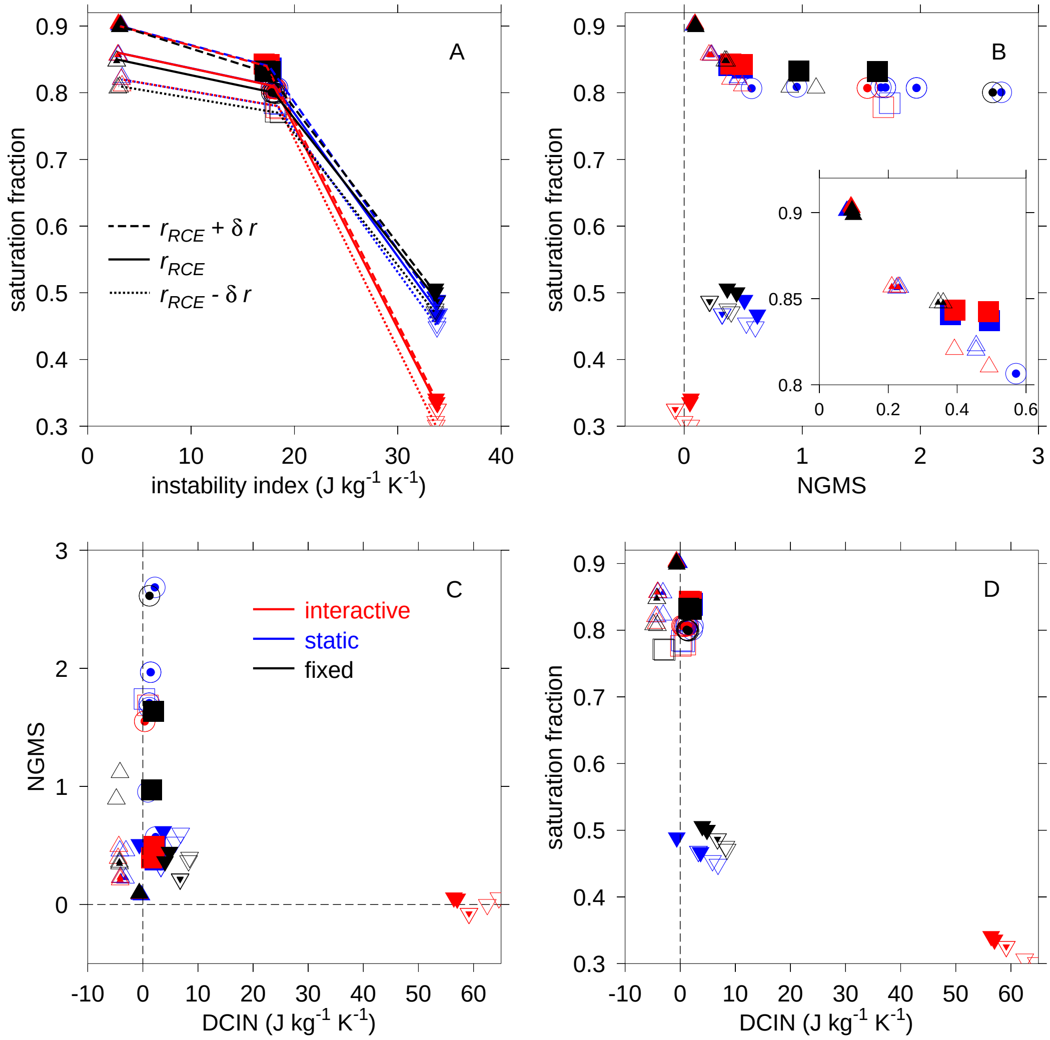

Figure 8. Relationships between convective diagnostics. (a) Saturation fraction versus instability index, (b) saturation fraction versus NGMS, (c) NGMS versus DCIN, and (d) saturation fraction versus DCIN. The symbol legend is the same as that in figure 7, colors represent radiation treatment. Lines in (a) connect experiments with identical reference moisture profiles. The inset in (b) is an amplification of (b) showing high saturation fractions and low NGMS.

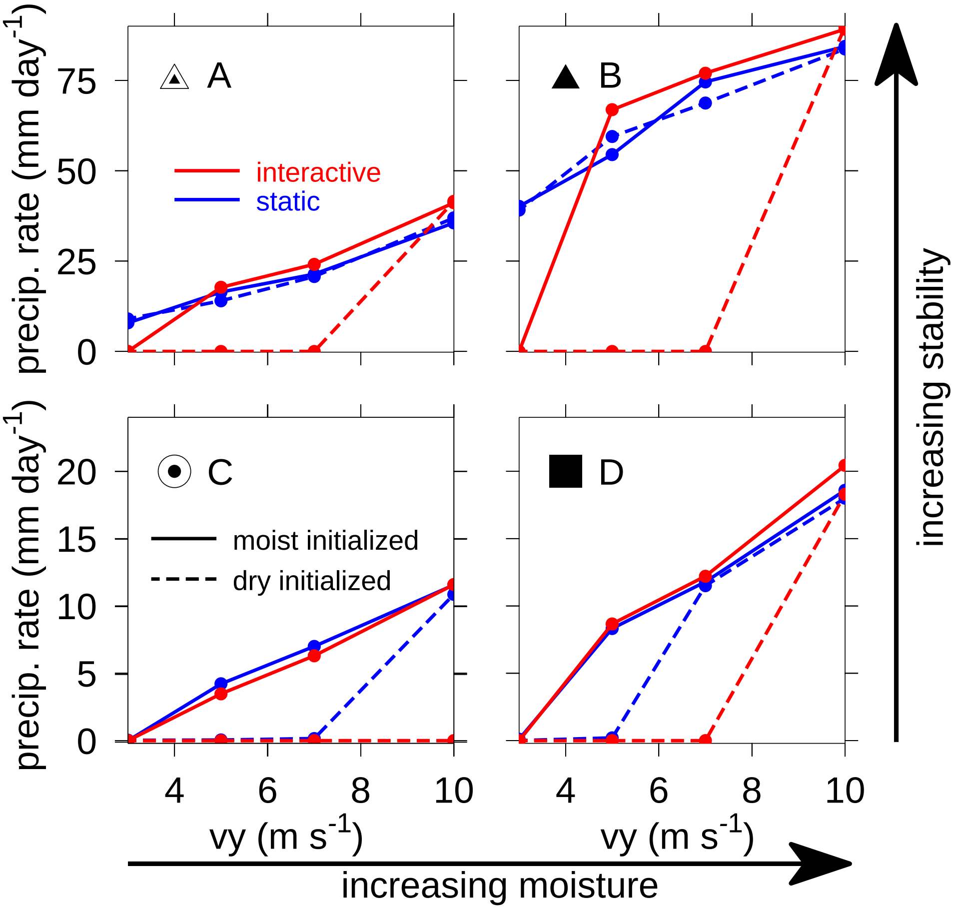

Figure 9. Precipitation rate as a function of surface wind speed, v_y, for different reference environments: (a) more stable, (b) more stable and moister, (c) unperturbed, and (d) moister. Solid lines correspond to simulations initialized with the reference moisture profile, dashed lines represent initially dry simulations. Blue lines are results for static radiation; red represents simulations with interactive radiation. Multiple equilibria exist when dashed lines show zero precipitation rate while solid lines have non-zero rates.

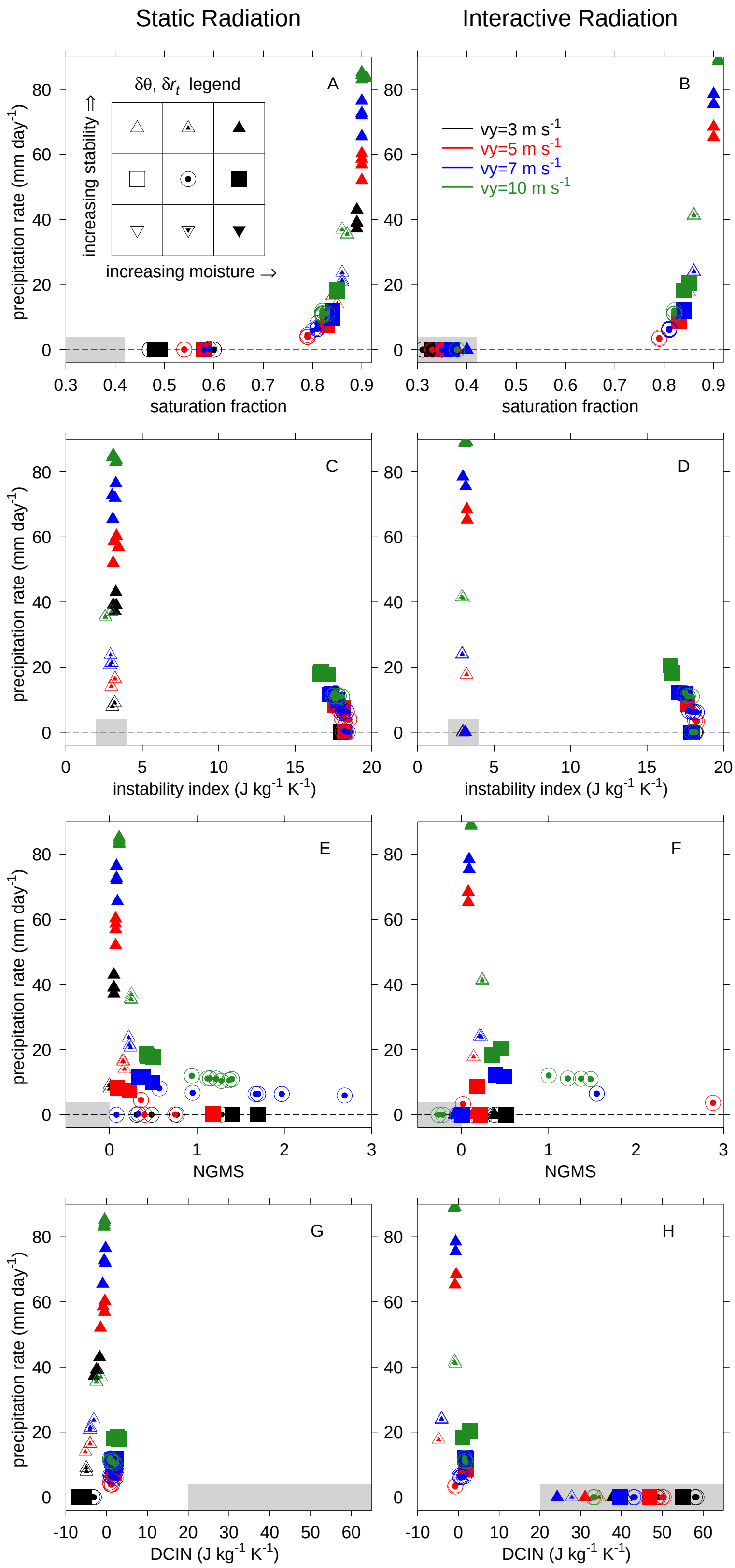

Figure 10. Scatterplots exhibiting the relationships between precipitation and (a,b) saturation fraction, (c,d) instability index, (e,f) NGMS, and (g,h) DCIN. Symbols

Figure 10. (continued)

correspond to the reference environments defined in figure 2, with a symbol legend as an inset in (a). Colors represent surface wind speeds used in each experiment. The left column (a,c,e,g) are results using static radiation; the right column (b,d,f,h) are results with interactive radiation. Significant differences between static and interactive radiation are highlighted with gray shading.